

The scaling relations of early–type galaxies in clusters

I. Surface photometry in seven nearby clusters

G. Fasano¹, D. Bettoni¹, M. D’Onofrio², P. Kjærgaard³, and M. Moles⁴

¹ Osservatorio Astronomico di Padova, Vicolo Osservatorio 5, I-35122 Padova, email: fasano@pd.astro.it, bettoni@pd.astro.it

² Dipartimento di Astronomia dell’Università di Padova, Vicolo Osservatorio 2, I-35122 Padova, email: donofrio@pd.astro.it

³ Copenhagen University Observatory. The Niels Bohr Institute for Astronomy, Physics and Geophysics
Juliane Maries Vej 30, DK-2100 Copenhagen, email: per@astro.ku.dk

⁴ Instituto de Matemáticas y Física Fundamental, CSIC, C/ Serrano 113B, 28006 Madrid, Spain, email: moles@imaff.cfmac.csic.es

Received December 2000

Abstract. This is the first paper of a series investigating the scaling relations of early–type galaxies in clusters. Here we illustrate the multi–band imagery and the image reduction and calibration procedures relative to the whole sample of 22 clusters at $0.05 \lesssim z \lesssim 0.25$. We also present the detailed surface photometry of 312 early–type galaxies in 7 clusters in the first redshift bin, $\approx 0.025\text{--}0.075$. We give for each galaxy the complete set of luminosity and geometrical profiles, and a number of global, photometric and morphological parameters. They have been evaluated taking into account the effects of seeing. Internal consistency checks and comparisons with data in the literature confirm the quality of our analysis. These data, together with the spectroscopic ones presented in the second paper of the series, will provide the local calibration of the scaling relations.

Key words. early–type galaxies – surface photometry – scaling relations

1. Introduction

Clusters of galaxies are the most massive, yet dynamically bound, known entities in the Universe. The identification of properties that could be universal would make them tracers of cosmic evolution since they can be detected at large distances. Indeed, the scaling relations satisfied by the global parameters of the early type galaxies, the dominant population in the densest parts of clusters, have become a powerful tool to elucidate the nature of the processes of formation and evolution of galaxies, as well as to perform different cosmological tests.

In general, assuming that early type (E or S0) galaxies of mass M and luminosity L , are in virial equilibrium, and that they all are homologous systems, it follows that some relation between size, surface brightness and velocity dispersion would be expected, provided that the M/L ratio is a function of the same variables. It is now well established that such a relation, the so called Fundamental Plane (FP hereafter), does exist (Dressler et al. 1987, Djorgovski & Davis 1987, Jørgensen, Franx and Kjærgaard 1995). It has the form $R_e \propto \sigma^\alpha \times I_e^\beta$, where R_e is the effective radius,

σ the velocity dispersion, and $\langle I \rangle_e$ the mean effective surface brightness.

The existence of the FP implies that the main physical relation governing the properties of E and S0 galaxies is just the virial condition (Faber et al. 1987). The precise form of the FP relation depends on different factors, such as the lack of exact homology of the early type galaxies in different contexts (i.e., differences in the luminosity profiles or in the dynamical structure: Caon et al. 1993, Graham et al. 1996, Ciotti et al. 1996) and the dependence of the M/L versus M relation on wavelength (Pahre and Djorgovski 1995; Pahre, Djorgovski, & de Carvalho 1998; Pierini et al. 2000; Mobasher et al. 1999). Moreover, it should be established which galaxies (i.e.: their luminosity range) are appropriate to build the FP. Given the number of factors that could contribute to the scatter of the FP, its small amplitude is remarkable. It is that small scatter which makes the FP an accurate distance indicator. The Kormendy relation, the projection of the FP onto the $R_e\text{--}I_e$ plane, has substantially more scatter. However, if part of that scatter could be understood in terms other than the velocity dispersion, its suitability for cosmological analysis could be reinforced. As discussed by Kjærgaard, Jørgensen

and Moles (1993; KJM hereafter), the rapidly increasing difficulty, for increasing cluster redshift, to obtain the velocity dispersion of a sizeable number of galaxies, results in defining the FP with rather limited samples, implying an increasing scatter.

In all the studies it is assumed that the Fundamental Plane, as well as its projections, the Kormendy relation in particular, are universal, in the sense of presenting the same coefficients everywhere, independently of any local property or even of the redshift. Indeed, it is the assumption of universality of the FP that could make it an appropriate tool in cosmology, e.g. in performing the Tolman test (KJM; Pahre, Djorgovski, & de Carvalho 1996; Moles et al. 1998), or to assess the evolution of M/L with z (Bender, Burstein, & Faber 1992; Guzmán, Lucey, & Bower 1993; van Dokkum and Franx 1996; Kelson et al. 1997; Jørgensen, & Hjorth 1997; Bender et al. 1998; Ziegler et al. 1999; Jørgensen et al. 1999; Kelson et al. 2000). This assumption, however, has to be empirically verified.

Jørgensen, Franx, & Kjærgaard (1996; hereafter JFK) have discussed the problem and presented a study of early type galaxies in ten clusters, finding that the distribution of their structural parameters can be fitted with a unique set of coefficients for all the clusters. However, as indicated by JFK, given the small sample size, in some cases, some variations of the order of 10% in the coefficients cannot be excluded. Their sample included clusters with a wide range of richness and regularity, with $z \leq 0.038$. Work at higher redshift (van Dokkum and Franx 1996) shows that the data can be consistently fitted with similar coefficients, but cannot be considered as definitive due to the small number of galaxies used to define the relations.

The program presented in KJM addresses the same question of the universality of the scaling relations, trying to separate the cosmic variance at a given redshift, from cosmic evolution effects in a systematic way. Our work includes galaxy clusters with a more restricted range of properties than in JFK, in the redshift range $0.035 \leq z \leq 0.28$, in 5 redshift steps. The comparison of the results for galaxy clusters at a similar redshift will allow to control the effects of local aspects of the evolution on the FP coefficients. Going to significantly higher redshift than JFK, we'll be able to test the behaviour of the scaling relations with z . We stress here that we not only consider in our program the FP relation, but, for the reasons pointed out before and discussed by KJM, we'll analyze the properties and behaviour of the Kormendy relation as well.

Another interesting aspect we want to study is the characterization of the family of galaxies that define and satisfy the scaling relations, an aspect not yet understood. Regarding the Kormendy relation, it is known that it is satisfied by only a fraction of early type galaxies in the (I_e - r_e) plane (Capaccioli, Caon, & D'onofrio 1992). It is one of our goals to analyze where the borderline of these two families lies, and the reason of such a dichotomy. Concerning the FP, even the deepest studies to now (Jørgensen 1999) only include the brightest end of the luminosity function,

as the measurement of the velocity dispersion of fainter early type galaxies needs of important amounts of observing time with very large telescopes.

The data we collected, following the scheme proposed by KJM, include surface photometry and spectroscopy (intermediate and low resolution) of a sizeable number of E and S0 galaxies in each cluster, to get not only the parameters $\langle I \rangle_e$, R_e and σ , but also a measure of the K-effect for each galaxy, together with their spectral energy distributions and some spectral indicators.

In the present paper, which is the first step to achieve such a program, we give an overview of all the photometric observations relative to the project, illustrating the sample selection and the observing strategy, describing the reduction and calibration of the data and discussing their quality (Section 2). We present here the detailed surface photometry of the galaxies, down to $M_r \sim -18.0$ mag ($H_0 = 75 \text{ km s}^{-1} \text{ Mpc}^{-1}$), for 7 nearby ($z \leq 0.075$) clusters of the sample (Section 3), describing the procedure we used to extract the global photometric and morphological parameters of galaxies (Sections 4,5). Finally we perform internal and external comparisons to check the reliability of our analysis (Section 6). The results on more distant clusters and the properties of the scaling relations will be given in following papers. Some preliminary results were anticipated in Fasano et al. (1997), and in Moles et al. (1998), where we have used the Kormendy relation to perform the Tolman surface brightness test. In Fasano et al. (2000) we have also presented the analysis of the morphological content (the E/S0/S fractions) in clusters up to $z \sim 0.5$, including some of our sample. Through this paper we assume $H_0 = 75 \text{ km s}^{-1} \text{ Mpc}^{-1}$ and $q_0 = 0.1$.

2. The global sample: observations and data reduction

2.1. Sample selection and cluster coverage

Table 1 lists the clusters in our sample and the observing runs in which they were observed (see next subsection). The clusters have been grouped in five redshift bins with step ~ 0.05 , from $z \sim 0.025$ up to $z \sim 0.25$. They were selected from the catalog by Abell et al. (1989) to be representative of massive, apparently relaxed systems, not too different from Coma, a regular cluster for which an important amount of relevant data is available. Thus we selected clusters of intermediate richness class, with Bautz-Morgan (1970) type II, II-III or III. Types I and I-II were excluded to avoid clusters dominated by a central, big cD galaxy. We also excluded those clusters with Rood-Sastry (1971) class L or I, to maximize the probability of dealing with virialized systems. Finally, we restricted the sample to rather high galactic latitudes (most have $|b| \geq 36^\circ$) in order to avoid problems with the extinction. The 22 clusters we actually observed (see Table 1) are from the resulting list, the final selection being a matter of opportunity. We notice that there is an exception to our selection criteria, namely A2670, a cD dominated cluster, BM class I-II.

Table 1. The global sample of clusters

Name	$\alpha(2000)^{(1)}$			$\delta(2000)^{(1)}$			z	BMtype ⁽²⁾	RStype ⁽³⁾	runs
A 2151	16 ^h	05 ^m	15 ^s	+17°	44′	55″	0.0365	III	<i>F</i>	2, 3
A 119	00	56	21	−01	15	47	0.0439	II – III	<i>C</i>	1, 5, 7
A 1983	14	52	44	+16	44	46	0.0456	III	<i>F</i>	3
DC 2103	21	08	37	−39	51	19	0.0527	–	–	4
A 3125	03	27	22	−53	30	38	0.0593	III	–	5
A 1069	10	39	54	−08	36	40	0.0630	III	<i>F</i>	5
A 2670	23	54	10	−10	24	18	0.0761	I – II	<i>cD</i>	7
A 3330	05	14	42	−49	03	00	0.0910	II	–	1, 5
A 2048	15	15	18	+04	22	00	0.0945	III	<i>C</i>	3
A 98	00	46	24	+20	29	00	0.1015	II – III	<i>F</i>	7
A 216	01	36	42	−06	24	00	0.1158	II – III	<i>C</i>	7
A 389	02	51	18	−24	54	00	0.1160	II	<i>F</i>	5
A 951	10	13	54	+34	43	00	0.1430	III	<i>B</i>	6
A 2235	16	55	00	+40	01	00	0.1511	III	<i>F</i>	7
A 1979	14	51	00	+31	16	00	0.1687	II – III	<i>F</i>	3
A 2658	23	45	00	−12	18	00	0.1850	III	<i>F</i>	3
A 2192	16	26	36	+42	40	00	0.1868	II – III	<i>F</i>	2, 3
A 1643	12	55	54	+44	04	00	0.1980	III	<i>B</i>	2
A 2111	15	39	36	+34	24	00	0.2290	II – III	<i>C</i>	2
A 2125	15	35	54	+70	03	00	0.2465	II – III	<i>B</i>	3
A 1952	14	41	06	+28	38	00	0.2480	III	<i>C</i>	3
A 1878	14	12	48	+29	12	00	0.2540	II	<i>C</i>	2

⁽¹⁾ NED coordinate⁽²⁾ Bautz – Morgan (1970) Type⁽³⁾ Rood – Sastry (1971) Class

The choice of the cluster fields to be observed in the framework of our global program is a more delicate question. The ideal approach would be to cover the whole cluster within ~ 1 Abell diameter. Indeed, for the determination of the FP, measuring the σ for substantially more than the ~ 15 –20 brightest early type galaxies in each cluster is too consuming in telescope time, and would require a separate observing program. On the other hand, to tackle the question of the family of galaxies actually defining the scaling relations, in particular the Kormendy relation, it would be necessary to have a fairly complete sample reaching some (faint) absolute magnitude limit. This is a program now under way, but for the time being we tried to optimize the effort making some compromises. Basically, for the nearest clusters (see Section 3) only individual targets were selected from the catalog by Dressler (1980) – the brightest E and S0 galaxies in his lists. Consequently only the galaxies entering the fields of those individual targets were recorded and measured (see Table 6). For more distant clusters the coverage approaches the ideal, since a substantial fraction of the whole cluster was sampled. The final data collection includes several dozens of galaxies per cluster with accurate surface photometry.

2.2. Observations and basic reductions

The observations for the whole sample of 22 clusters were collected from Dec. 1994 to Aug. 1998 with the Nordic

Optical Telescope (NOT, La Palma) and with the 1.5m Danish telescope at La Silla (Chile). Images have been obtained in two or three bands [Gunn r (r), Bessel V (V) and Bessel B (B)] to provide the color term of each object. Moreover, as a general strategy, at least two exposures for each field in each filter were usually taken, allowing us to clean-up the combined images for cosmic-rays.

In Table 2 we report the log of observations, together with the basic information about the instrumentation. In each observing run, besides the cluster fields, a number of nearby standard galaxies were imaged in the above mentioned bands, thus allowing internal and external check of the surface photometry (see Section 6).

Dark counts with different exposure times were obtained in each run and turned out to be negligible. For the bias, several frames were recorded every night to check the stability of the corresponding frame structure. We also obtained, every night, several flat field (FF), twilight sky exposures which, after comparison, were used to derive an average frame. Apart from run #5, the quotient frames obtained using FFs relative to different nights of the same run, turned out to be almost flat, allowing us to produce a grand-averaged, high S/N ratio FF to be used for the whole run.

The typical uncertainties associated with the reduction procedures are of few tenths of ADU (0.1–0.2) for the bias removal and of few thousandths of the background (0.001–0.006) for the flat fielding. These uncertainties, to-

Table 2. Observing Runs

Run	Date	Telescope	Camera	CCD	readnoise (<i>e</i>)	gain (<i>e</i> /ADU)	PixelScale (<i>''</i> / <i>pixel</i>)	F.O.V. <i>arcmin</i> × <i>arcmin</i>
1	Dec. 4 – 8 1994	1.5Danish	DFOSC	Thompson	3.70	2.00	0.510	8.7 × 8.7
2	May 24 – 27 1995	NOT	StanCam	Tektronik	6.36	1.69	0.176	3 × 3
3	Jun. 23 – 26 1995	NOT	StanCam	Tektronik	6.36	1.69	0.176	3 × 3
4	Sep. 19 1995	1.5Danish	DFOSC	Loral	4.90	1.31	0.390	13.4 × 13.4
5	Jan. 1 – 8 1997	1.5Danish	DFOSC	Loral	4.90	1.31	0.390	13.4 × 13.4
6	Feb. 27 – 28 1997	NOT	ALFOSC	Ford – Loral	6.50	1.02	0.189	6.5 × 6.5
7	Aug. 29 1998	NOT	ALFOSC	Ford – Loral	6.50	1.02	0.189	6.5 × 6.5

gether with those relative to the photometric calibration (see Table 3), will be used in Section 5 to evaluate the expected errors in the global photometric and morphological parameters.

During run #1 we used DFOSC during its testing phase, paying this choice with some instability of the acquisition system. The most serious drawback was the unreliability of the header content, including the exposure time and the zenith distance. In the next subsection we will report on the problems caused by this fact in the calibration procedure.

Runs #2 and #3 were characterized by exceptional weather conditions. All the nights were photometric and the seeing turned out to be permanently and largely below one arcsecond, with a minimum value around 0^{''}.45 (run #2, May 24 1995).

During the run #5 the seeing was mediocre (1^{''}.3–1^{''}.5). We had six photometric nights grouped in two intervals (Jan. 1–3 and 6–8), which turned out to be slightly different as far as the reduction and calibration parameters are concerned (see Table 3).

2.3. Calibration to standard passbands

During each observing night, several (from 30 to 60) standard stars from Landolt (1992), Jørgensen (1994) and Montgomery et al (1993), were observed at different zenith distances. In some cases the standard stars exposures were slightly defocused to avoid saturation of the brightest stars. The radius for the aperture photometry was set to 3.5 × FWHM, where the FWHM includes the possible effect of defocusing.

The coefficients of the relations between instrumental magnitudes in the *i*th band, $m_i^{raw} = -2.5 \log(\text{counts}/\text{sec})$, and the standard systems have been computed adopting general expressions of the form:

$$K_i = m_i^{std} - m_i^{raw} = C_0^i + C_c^i(ij) \times col_{ij}^{std} + C_z^i \times sec(z_d) \quad (1)$$

where m_i^{std} is the standard magnitude in the *i*th band, $col_{ij}^{std} = (m_j^{std} - m_i^{std})$ is the color of the object in the standard system, z_d is the zenith distance and C_0^i , $C_c^i(ij)$, C_z^i are the night constant, the color coefficient and the extinction coefficient, respectively.

The coefficients C_0^i and C_z^i depend on the observing conditions (basically on the site and on the night), whereas the color coefficient $C_c^i(ij)$ should only depend on the filter (*i*) and on the color (*ij*) since it indicates how well the instrumental response (telescope+filter+detector) matches the adopted standard system.

Since in each given run we found similar extinction coefficients for the nights when we did photometry, in order to derive the calibration coefficients we adopted the following multistep procedure:

(i) for each run and filter, the instrumental magnitudes of individual stars observed at different zenith distances were compared with the corresponding magnitudes in the standard system in order to determine a ‘run-averaged’ extinction coefficient; (ii) for each night and for each filter, the extinction coefficients were used to determine the night zero-point offsets; (iii) for each filter, the ‘zero-airmass’ calibration coefficients, reduced to a common offset, were then correlated with the standard colors to get the color coefficients and the ‘common offset’ zero points; (iv) for each night and for each filter, the final zero point was obtained by adding the night offset to the corresponding ‘common offset’ zero point.

Since we did *r* band observations in all runs, we report in Table 3 the best-fit values of the coefficients K_r for each observing night, together with the relative uncertainties and the final r.m.s.

A special case is that of the run #1 due to the incompleteness of the header information (see Section 2.2). The large uncertainties relative to this run in Table 3 reflect these calibration problems. For the time being we present here just the results from a field which overlaps with other field observed in a different run. The complete photometry of run #1 will be presented separately in a forthcoming paper.

3. The sample of early-type galaxies in nearby clusters

In the following we will concentrate on the surface photometry of early type galaxies in the seven clusters of Table 1 belonging to the first redshift bin ($z \lesssim 0.075$). The results of the present analysis will be used in a forthcoming

Table 3. Calibration coefficients and errors in the r band

Run	Night(s)	Color	C_0	C_c	C_z	r.m.s.
1	Dec. 4	$(B-r)$	22.802 ± 0.019	0.110 ± 0.018	-0.087 ± 0.023	0.058
1	Dec. 4	$(V-r)$	22.866 ± 0.015	0.342 ± 0.024	-0.087 ± 0.023	0.060
2	May 24	$(B-r)$	24.737 ± 0.007	0.085 ± 0.003	-0.128 ± 0.013	0.021
2	May 25	$(B-r)$	24.704 ± 0.004	0.085 ± 0.003	-0.128 ± 0.013	0.022
2	May 26	$(B-r)$	24.738 ± 0.005	0.085 ± 0.003	-0.128 ± 0.013	0.027
2	May 27	$(B-r)$	24.755 ± 0.006	0.085 ± 0.003	-0.128 ± 0.013	0.031
3	June 23	$(B-r)$	25.123 ± 0.015	0.117 ± 0.005	-0.088 ± 0.005	0.022
3	June 24	$(B-r)$	25.123 ± 0.009	0.117 ± 0.005	-0.088 ± 0.005	0.030
3	June 25	$(B-r)$	25.111 ± 0.005	0.117 ± 0.005	-0.088 ± 0.005	0.023
3	June 26	$(B-r)$	25.121 ± 0.008	0.117 ± 0.005	-0.088 ± 0.005	0.036
4	Sep. 19	$(V-r)$	21.357 ± 0.021	0.467 ± 0.089	-0.081 ± 0.003	0.020
5	Jan. 1–3	$(B-r)$	23.619 ± 0.003	0.075 ± 0.003	-0.105 ± 0.030	0.015
5	Jan. 6	$(B-r)$	23.569 ± 0.001	0.075 ± 0.003	-0.105 ± 0.030	0.015
5	Jan. 7	$(B-r)$	23.631 ± 0.001	0.075 ± 0.003	-0.105 ± 0.030	0.015
5	Jan. 8	$(B-r)$	23.663 ± 0.001	0.075 ± 0.003	-0.105 ± 0.030	0.015
5	Jan. 1–3	$(V-r)$	23.696 ± 0.001	0.187 ± 0.008	-0.105 ± 0.030	0.014
5	Jan. 6	$(V-r)$	23.646 ± 0.001	0.187 ± 0.008	-0.105 ± 0.030	0.014
5	Jan. 7	$(V-r)$	23.708 ± 0.001	0.187 ± 0.008	-0.105 ± 0.030	0.014
5	Jan. 8	$(V-r)$	23.740 ± 0.001	0.187 ± 0.008	-0.105 ± 0.030	0.014
6	Feb. 27	$(B-r)$	25.285 ± 0.005	0.074 ± 0.004	-0.084 ± 0.005	0.021
6	Feb. 28	$(B-r)$	25.321 ± 0.005	0.074 ± 0.004	-0.084 ± 0.005	0.022
7	Aug. 29	$(B-r)$	25.264 ± 0.009	0.124 ± 0.008	-0.090 ± 0.003	0.027

paper to investigate the properties of the galaxy scaling relations in nearby clusters (see Section 1).

In column 1 of Table 4 we list the clusters ordered by increasing redshift, while columns 2 to 4 report, for each cluster, the galactic extinction given by Schlegel et al. (1998; see Jørgensen et al. 1994 for conversion to the r band).

As explained in the previous section, the observations relative to the present sample of nearby clusters have been done in different observing runs, using different telescopes and different CCD cameras (see Table 2). In most cases it was not possible to secure a systematic coverage of the cluster area. In particular, for clusters observed only during the runs #2 and #3 (A2151 and A1983; detector field of view $\sim 3' \times 3'$), only a few galaxies per frame were registered.

The size and the location of the fields inside the cluster areas are shown in Figures 12a,...,g. In these figures each field color refers to a given telescope+camera equipment (see caption) and the grid sizes in right ascension and declination are of $30''$ and $5'$, respectively. In Table 6 the list of the imaged fields for each cluster is reported in ascending order of declination (see pointing coordinates in columns 4 and 5) and each field is identified by a letter (column 2). In the same table the seeing (column 6) and the relative uncertainty of the background (column 7; see Section 4.1) are reported.

3.1. Selection of galaxies

Even if the available imaging did not allow us to deal with complete samples of galaxies as far as the cluster coverage is concerned, we decided to set the absolute magnitude limit $M_r^{lim} = -18$ mag for inclusion in the final sample, in order to provide homogeneous data to study the Kormendy relation in a consistent way. That luminosity limit represents a compromise between depth of the sampling and the possibility to perform a detailed morphological analysis. The corresponding limits in apparent magnitude, r_{lim} , given our choice of cosmology (see Section 1) and taking into account the proper galactic extinctions (see Table 4), are given in column 5 of Table 4.

The automatic tool SExtractor (Bertin and Arnouts 1996) was used to produce preliminary galaxy catalogs from the images in the r band, allowing also an easy identification and rejection of stars. The preliminary catalog contained galaxies of all morphological types, down to SExtractor magnitudes $r_{lim} + 0.5$ mag. The additive factor 0.5 mag represents an upper limit of the bias affecting SExtractor magnitudes of early-type galaxies (Fasano and Filippi 1998, Franceschini et al. 1998). It prevented faint galaxies with lower average surface brightness from being excluded *a priori* from the sample.

The images were then processed by the automatic surface photometry tool *GASPHOT* (Pignatelli and Fasano 1999) to produce a first version (rough but fast) of the luminosity and geometrical profiles of the selected galaxies. These were used as a powerful complement to the visual inspection with the IRAF-*imexamine* tool in estimating the morphological types, allowing us to retain

Table 4. The nearby cluster sample

Cluster	$A_B^{(1)}$	$A_V^{(1)}$	$A_r^{(1)}$	$r_{lim}^{(2)}$	$N_{gal}^{(3)}$	$n_z^{(4)}$	$n_{dz}^{(5)}$	$n_{red}^{(6)}$	$n_{field}^{(7)}$
A 2151	0.205	0.158	0.128	17.86	37	23	2	3	1
A 119	0.167	0.128	0.104	18.26	57	27	2	1	4
A 1983	0.114	0.088	0.071	18.35	46	21	3	12	1
DC 2103	0.176	0.130	0.110	18.67	49	20(15)	7	1	5
A 3125	0.068	0.052	0.042	18.93	80	29(5)	4	5	15
A 1069	0.175	0.134	0.109	19.07	56	18(6)	3	3	15
A 2670	0.187	0.144	0.117	19.49	36	27	1	2	1

⁽¹⁾ galactic extinction (mag) in the B, V, and r bands

⁽²⁾ limiting r magnitudes for inclusion in the sample

⁽³⁾ number of early – type galaxies before membership control

⁽⁴⁾ number of available redshifts (our measurements in parenthesis)

⁽⁵⁾ number of galaxies which are not cluster members

⁽⁶⁾ number of galaxies redder than the cutoff lines in Fig.1

⁽⁷⁾ expected number of background and field galaxies

in the catalog only galaxies classified as E or S0. Our classification scheme is not based on quantitative morphology. However it is worth noticing that, relying on the same observational material presented here, we give in Fasano et al. (2000) the morphological type of galaxies in nine clusters with $0.1 \leq z \leq 0.25$. In that paper it is shown that our classification scheme turns out to be a robust one, both in an absolute sense and relative to the scheme by Dressler et al. (1997). In column 6 of Table 4 the number of galaxies after this preliminary selection is reported for each cluster. Moreover, in column 3 of Table 7 we give the morphological type of the galaxies in the final sample.

3.2. Cluster membership

The next step was to evaluate the cluster membership of the galaxies in our catalogues. The definitive criterion is indeed the redshift, so we searched the literature for the redshift information relative to our low redshift clusters. To the collected 147 redshifts we have to add the 26 new redshifts that were obtained in the framework of our long-term project aimed at measuring line strengths of galaxies in nearby clusters (136 low resolution spectra of galaxies in 11 nearby clusters; Moles et al. 2001, in preparation). In column 7 of Table 4 we report, for each cluster, the total number of available redshifts, while the number of redshifts derived from our spectra are reported in parenthesis. The number of galaxies which are not cluster members ($|cz - \langle cz \rangle| \geq 2500$) in each cluster is reported in column 8 of Table 4.

Since redshift determinations are usually available only for $r \lesssim 16$, we tried the color–magnitude relations (*CMR*) to eliminate some red objects, presumably background galaxies. The package SExtractor was again used to derive the instrumental colors using apertures corresponding to a rest-frame radius of ~ 5 kpc. Then, the standard ($B - r$) and/or ($V - r$) colors were derived, depending on

the bands in which each cluster (or even each field) had been imaged.

In Figure 1 we present the *CMRs* of the 7 clusters, together with the red cutoff lines we used for the membership acceptance. These were obtained shifting the average *CMRs* we derived from the literature by an arbitrary factor (0.2) accounting for both the intrinsic scatter of the *CMRs* (~ 0.1) and the expected uncertainties in the magnitude estimates of SExtractor (~ 0.1 in r and ~ 0.2 in B and V). The average *CMRs* in the left part of Figure 1 ($B - r$ vs. r) were derived adopting for the slope the fixed value of -0.03 , obtained from the data in Jørgensen et al. (1995; see also Gladders et al. 1998). The zero points as a function of redshift were computed according to the equation given in Yee et al. (1999) and using the transformations to the Gunn system provided by Jørgensen (1994). The same transformations were used to derive the slope and the zero points for the ($V - r$)– r relations (right part of the figure). All the galaxies in each cluster redder than the corresponding cutoff line were excluded from the final sample; they are reported in column 9 of Table 4. The full/open dots in the figures represent galaxies with/without measured redshift, while the crosses indicate galaxies which, according to the redshift criterion, are not cluster members. Notice that we do not use any cut-off in the blue side to avoid arbitrarily eliminating genuine blue galaxies. We stress that we don't use the *CMR* as real membership discriminator, but only as a tool to eliminate those galaxies most likely in the background of the cluster.

In column 10 of Table 4, for each cluster (with the proper area coverage and limiting magnitude) we report the expected background and field contamination obtained using the galaxy number counts given by Metcalfe et al. (1995) and assuming the canonical breakdown into morphological classes given for the field by Dressler (1980; E:S0:Sp+Irr = 10:10:80). Table 4 (see also Figure 1) shows that, in all clusters but Abell 1983, the

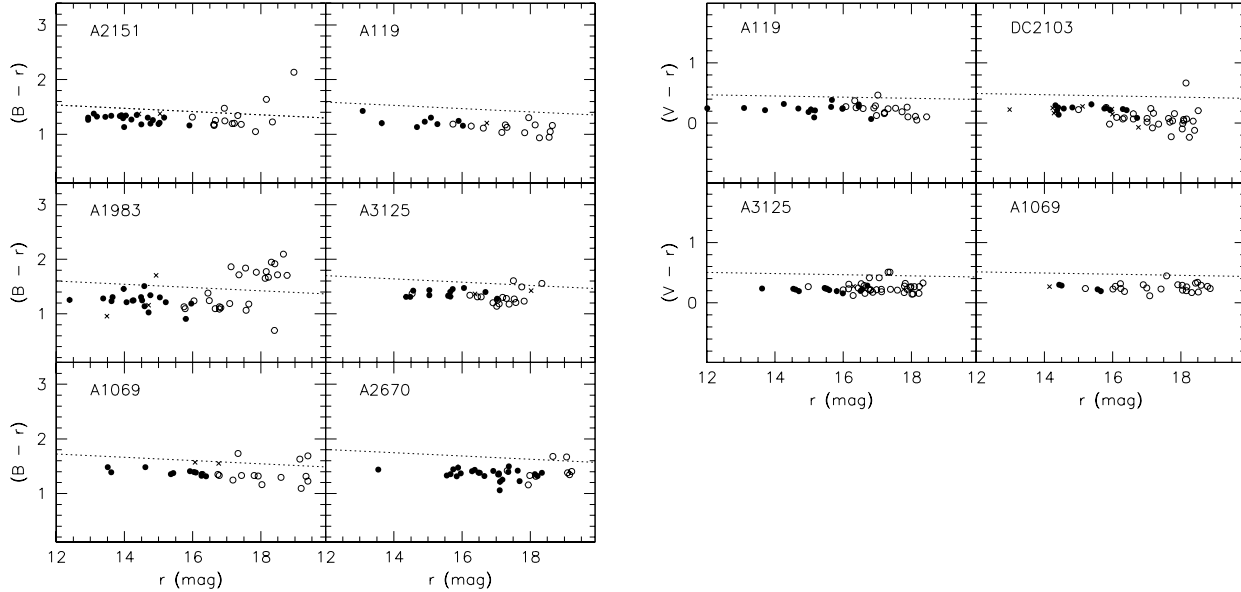


Fig. 1. Color-magnitude relations $(B - r) - r$ and $(V - r) - r$ for the nearby clusters. The dotted lines represent the upper limits we adopted for inclusion in the final catalog (see text). Full and open circles indicate galaxies with known and unknown redshift, respectively. Crosses represent galaxies which, according to the above redshift criterion, are not cluster members (see text).

expected number of background and field galaxies agrees, within the Poissonian uncertainty, with the total number of objects excluded from the sample due to redshift and/or color discrepancy. The sizeable number of faint, red galaxies in Abell 1983 could indicate the presence of some background galaxy concentration.

In the Figures 12a,...,g the selected galaxies are marked by small circles, whereas the corresponding Figures 13a,...,g show the detailed maps of the fields, the galaxies being numbered in ascending order of declination for each field. In this way each galaxy in our sample is identified by the cluster name, the field letter and the galaxy number. In Tables 7a,...,g we report, for each cluster, the galaxy sample for which accurate surface photometry has been achieved.

4. Surface photometry

Detailed surface photometry was obtained using the *AIAP* package running at the Padova Observatory (Fasano 1990), which allows to derive photometric and structural profiles of individual galaxies. The advantages of using this software have been presented elsewhere (i.e. Fasano et al. 1996). We note that, due to its high degree of interactivity, the *AIAP* package turns out to be particularly useful for analyzing the isophotes of galaxies embedded in high density regions, such as rich clusters or compact galaxy groups.

4.1. Ellipse fitting profiles

The surface photometry was always accomplished on the r images, apart from that relative to the observations of A119 during the runs #1 and #5 (33 galaxies), for which the images in the V band turned out to be deeper.

Before starting the analysis of individual galaxies, each frame was handled in order to achieve a careful sampling, fitting and removal of the sky. Apart from a few cases, a two-dimensional, first-degree polynomial was sufficient to give an accurate fit to the sky. The distribution of the residuals in the frame was used to estimate the relative uncertainty of the sky level ($\Delta_{\text{sky}}/\text{sky}$; see column 7 in Table 6), which has influence on the errors of the profiles and on the global parameters.

In each *AIAP* run we sliced the galaxy image with a fixed step in surface brightness (0.2 mag), we fitted the isophotes with ellipses and we produced a set of profiles (surface brightness μ , coordinates of the center, ellipticity ε , position angle θ and coefficients of the Fourier analysis of the residuals) as a function of the semi-major axis a_{maj} of the ellipses. Following Fasano and Bonoli (1990), the error estimates of luminosity, ellipticity and position angles profiles were derived taking into account the *FWHM* and the above mentioned uncertainty of the sky level.

The errors of the Fourier coefficients were estimated from the local noise of the profiles. To illustrate what kind of information we are dealing with, we report in Figure 2 two examples of *AIAP* profiles, the first one referred to an elliptical galaxy (A2151-f1), the other one to an S0 galaxy (A1069-a3). The complete set of profiles (Tables and Figures) for the whole galaxy sample is available in

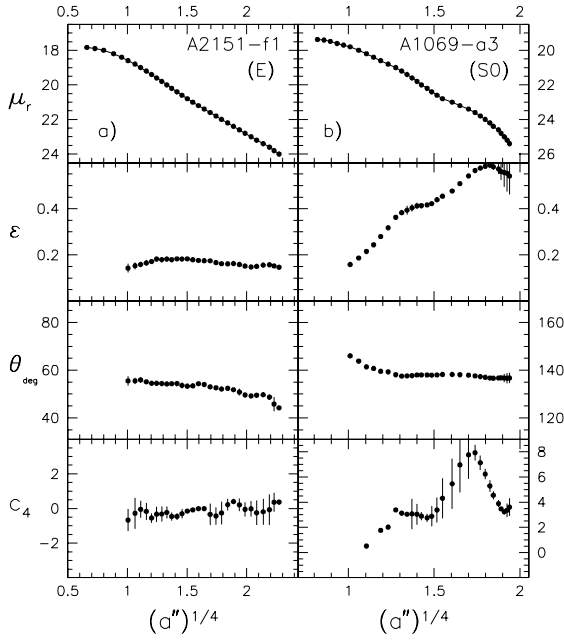


Fig. 2. Examples of luminosity and morphological profiles extracted using *AIAP*: *a*) a typical elliptical galaxy (A2151-f1) and *b*) a typical S0 galaxy (A1069-a3).

electronic form. We note that, for historical reasons, the position angles in the Tables (see also Tables 7a,...,g) are counted clockwise from the North, while in the figures (see also Figure 2) they are counted counter-clockwise (again from the North).

4.2. Provisional magnitudes and metric sizes

The global parameters of galaxies have been mostly extracted from the equivalent luminosity profiles, which give the surface brightness as a function of the isophotal equivalent radius $R_{eq} = a_{maj} \sqrt{1 - \varepsilon}$.

Estimating the total magnitude m_T of elliptical galaxies is known to be a rather difficult task, particularly in the cores of rich clusters. The light distribution of elliptical galaxies smoothly decreases outwards and it is practically impossible to establish the galaxy bounds. The problem is two-fold: first, an extended aperture photometry turns out to be unfeasible in the crowded galaxy fields typical of the cluster cores; and, on the other hand, due to the rapidly decreasing S/N ratio, usually the luminosity profiles obtained from ellipse fitting of the isophotes cannot be extended to approach the true value of the total magnitude close enough. This makes some extrapolation unavoidable.

Our strategy in estimating the provisional values of the total galaxy magnitudes was the following: (*a*) for $R_{eq} > 3 \times FWHM$, the luminosity profiles were tentatively fitted with a generalized de Vaucouleurs law $\mu(R) = \mu_0 + C(n) \times (R/R_e)^{1/n}$ (Sersic 1968, Ciotti 1991, Caon

et al. 1993), providing a first guess of the parameter n . To each profile fitting we assigned arbitrarily a quality index Q (good fit: $Q=1$) that takes into account the problems encountered during the fit (such as the presence of undulations, bumps, etc.) and during the data reduction (the galaxy was in a crowded region, or near the boundaries of the chip, etc.); (*b1*) in case of good fit ($Q=1$), the $R^{1/n}$ law was used to extrapolate the luminosity profile in order to derive the total magnitude; (*b2*) if the fit was not satisfactory in spite of the large angular size and brightness of the galaxy (luminosity profile intrinsically not performable by a $R^{1/n}$ law, i.e. S0s with bulge+disk profiles, bright extended halos, etc..) the extrapolation was achieved using the de Vaucouleurs $R^{1/4}$ law or the exponential law, depending on the shape of the outer part of the profile; (*b3*) if the fit was not good due to the small size and/or low brightness of the galaxy, the total magnitude was computed by averaging the luminosities derived by the $R^{1/4}$ and exponential extrapolations of the luminosity profile.

In order to give model independent estimates of the scale radius of galaxies, as well as of the average surface brightness inside that radius (both to be used in the scaling relations), we decided not to use the effective radius R_e defined by the slope of the $R^{1/n}$ law representation of the luminosity profile. Instead, we preferred to use the half-light radius R_{50} , defined as the equivalent radius enclosing half of the total galaxy light, and the corresponding average surface brightness $\langle \mu_{50} \rangle$. We also derived from the equivalent luminosity profile of each galaxy the radius R_{75} corresponding to 75% of its total luminosity (together with the corresponding average surface brightness $\langle \mu_{75} \rangle$) and the Petrosian (1976) radii R_{P139} and R_{P200} , corresponding to the radii for which the difference $\mu - \langle \mu \rangle$ (local minus average surface brightness) is 1.39 and 2.00, respectively. We refer the reader to KJM for an exhaustive discussion of the features of the Petrosian metric sizes. Here we remind that, in case of a perfect de Vaucouleurs luminosity profile, the Petrosian radii R_{P139} and R_{P200} coincide with R_{50} and R_{75} , respectively.

4.3. Luminosity profile restoration

The study of the Kormendy relation of early type galaxies in clusters requires accurate estimates of some metric radius R_m and of the average surface brightness inside that radius $\langle \mu_m \rangle$. In Fasano et al. (1997) it is illustrated, for two clusters at $z \sim 0.25$ (A2111 and A1878), the crucial role played by the deconvolution of the luminosity profiles in recovering the global parameters R_{50} and $\langle \mu_{50} \rangle$ from ground-based material (even of excellent quality). The redshift of the clusters in the present sample is smaller, but the correction is still important for the faint (and small) end of the galaxy population, for which the values of R_m and $\langle \mu_m \rangle$ derived directly from the observed luminosity profiles can be strongly affected by the seeing.

As in Fasano et al. (1997), we used the Multi-Gaussian Expansion deconvolution technique (*EMGDEC*,

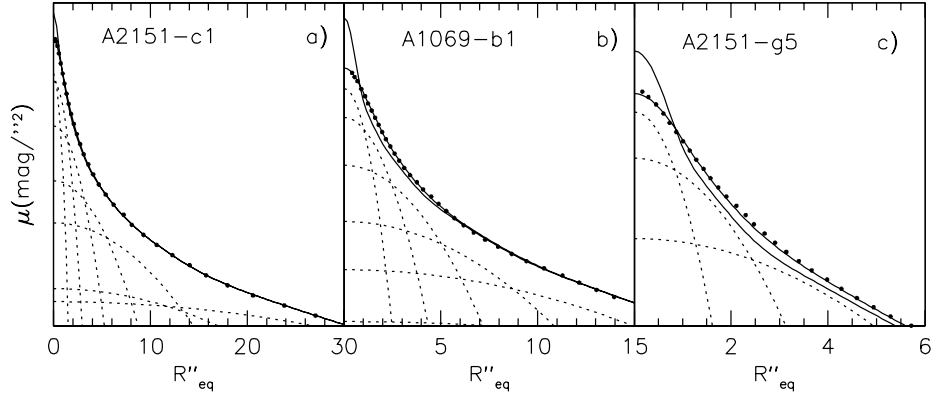


Fig. 3. Examples of *EMGDEC* deconvolution: *a*) a large galaxy (A2151-c1), *b*) a medium size galaxy (A1069-b1) and *c*) a small galaxy (A2151-g5). The full dots represent the luminosity profiles extracted by *AIAP* and interpolated by means of suitable multi-gaussian expansions (dotted lines). The steeper (full) lines represent the deconvolved luminosity profiles. The surface brightness is in arbitrary units.

Bendinelli 1991) to achieve the luminosity profile restoration. The input data of the *EMGDEC* algorithm are the equivalent luminosity profiles of the galaxy and of the *PSF*, both represented in analytical form by means of suitable series of gaussians. Although using a parametric approach, *EMGDEC* has the advantage of a very accurate representation of the luminosity profiles. In Figure 3 we show some examples of *EMGDEC* restoration applied to the luminosity profiles of galaxies belonging to our sample and spanning a wide range in size. Obviously for large galaxies, only the inner part of the profile is modified by *EMGDEC*, while for small galaxies the restoration affects the whole profiles. We emphasize that in any case the convolution of the restored luminosity profiles perfectly reproduces the profiles actually observed.

It is worth noticing that the *EMGDEC* deconvolution is not unique, the result depending on the multi-gaussian representation (and extrapolation) of the profiles, as well as on the so called regularization tool (see Bendinelli 1991 for details). In order to check the reliability and the robustness of the deconvolved half-light radii we have analysed a sample of 64 toy galaxies with ellipticity $\varepsilon=0$, Sersic's indexes $n=1$ and $n=4$ and half-light radii spanning the range $R_{50}^{true}/FWHM=0.5-5$. The simulated frames reproduces the typical conditions of our observing runs #2 and #3, including the background noise. The luminosity profile of each toy galaxy was deconvolved nine times changing both the number of gaussians used to represent it (3 to 5) and the regularization coefficient of *EMGDEC* (0.0001, 0.001 and 0.01). In Figure 4 we report, for each toy galaxy, the average value (together with the relative *r.m.s.*) of the difference between estimated and true values of the half-light radius as a function of the true value itself. We conclude that, at least for circularly symmetric objects, the *EMGDEC* tool produces un-biased values of the deconvolved half-light radii and

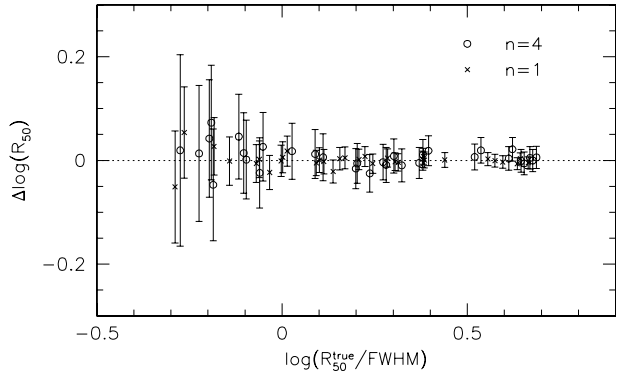


Fig. 4. Difference between estimated and true value of the average half-light radius as a function of the true value itself for a sample of 64 toy galaxies (see text for details on the simulation). The open circles refer to toy galaxies with de Vaucouleurs luminosity profiles, while crosses refer to exponential luminosity profile galaxies.

that, changing the starting conditions within wide ranges produces only marginal changes in the half-light radius down to $R_{50} \simeq FWHM$.

Since the *EMGDEC* algorithm only deals with circularly symmetric objects, we have carried out numerical simulations of galaxies with different flattening in order to explore how the ellipticity influences the *EMGDEC* equivalent profile restoration, in particular as far as the Sersic's index, the effective radius and the corresponding average surface brightness estimates are concerned. Figure 5 illustrates the results for a sample of 64 elliptical ($n=4$) or disk ($n=1$) toy galaxies having faint magnitudes (17.5-18.5 mag) and small effective radii (5-9 pixels). Again, the simulated frames reproduces the typical condi-

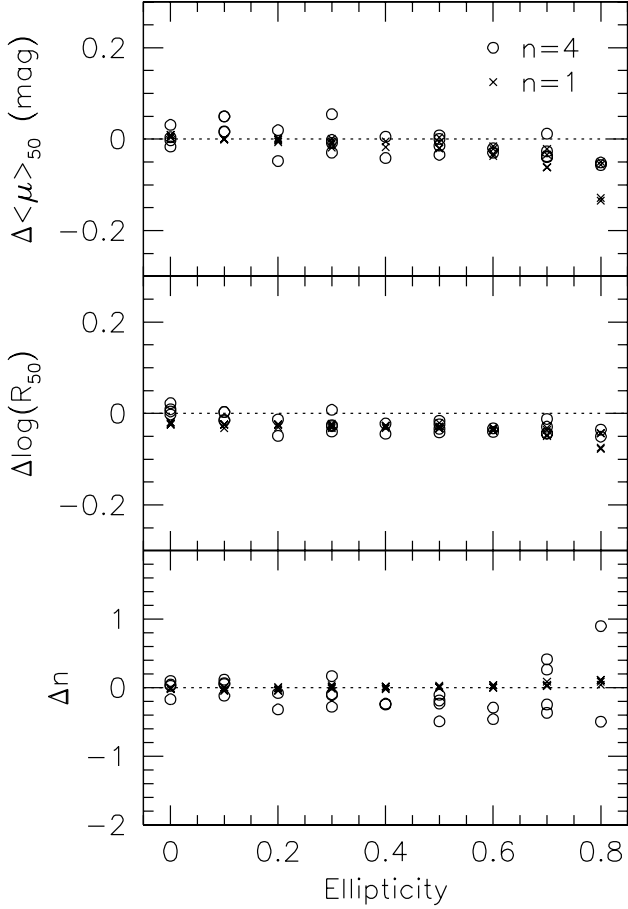


Fig. 5. Difference between estimated and true values of the average half-light surface brightness, half-light radius and Sersic's index, after *EMGDEC* restoration, for a sample of 64 toy galaxies (see text for details on the simulation). The open circles refer to toy galaxies with de Vaucouleurs luminosity profiles, while crosses refer to exponential luminosity profile galaxies.

tions of our observing runs #2 and #3. We conclude that the influence of the isophotal flattening on the estimation of the equivalent parameters after *EMGDEC* restoration is relatively unimportant except for an ellipticity greater than 0.7.

5. Global parameters and errors

We have used the restored, *equivalent* luminosity profiles to derive the final values of the global parameters related to magnitudes and metric sizes, as well as to compute the final value of the Sersic's index n . The other '*globals*' related to the morphology (ϵ , θ and Fourier coefficients) have been derived from the original profiles, since our one-dimension technique of restoration is not able to recover the '*true*' galaxy geometry.

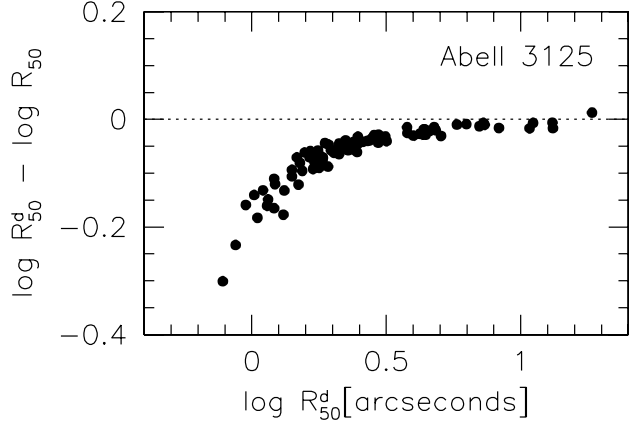


Fig. 6. Difference between half-light radii before and after deconvolution of the luminosity profiles for the galaxies in Abell 3125.

5.1. Final magnitudes and metric sizes

The same strategy as outlined in Section 4.2 to estimate the *provisional* total magnitudes from the raw luminosity profiles, was used to estimate the final total magnitudes from the de-convolved luminosity profiles (columns 7 of Tables 7). In this case we have adopted a fixed range of R/R_{50} (0.15 to 4, with a minimum allowed angular radius of $0''.5$) to produce χ^2 fits of the luminosity profiles, leading to the final values of the Sersic's parameter n . Since the value of R_{50} depends on the total magnitude itself, a two-step iterative procedure was necessary. We note that, if the quality of the fit is good ($Q = 1$, case [b1]), the total magnitude m_T was derived extrapolating the observed luminosity profile by a generalized de Vaucouleurs law with index n . Otherwise (cases [b2] and [b3] in Section 4.2) the $R^{1/4}$ and/or the exponential laws were used for the extrapolation.

The final values of the different metric sizes mentioned in Section 4.2, together with the corresponding average surface brightness, were easily derived from the restored luminosity profiles, once the total magnitudes were known. It is worth mentioning that the restored values of the total magnitude differ only slightly from the corresponding ones provisionally derived from the raw luminosity profiles. On the contrary, the restoration procedure deeply influences the different kinds of metric radius, as well as the corresponding average surface brightness.

As an example, in Figure 6 the difference between restored and raw values of R_{50} for the galaxies in A3125 is reported as a function of R_{50} . The same qualitative behaviour is found for all clusters, with systematic differences mainly depending on the seeing, on the pixel-size and on the S/N ratio, and individual differences due to the shape of profiles.

In order to give realistic estimates of the uncertainties associated to total magnitude, metric radius and average surface brightness, we have taken into account all the possible sources of error. The contribution due to the standard calibration includes all the uncertainties related to the color term and to the atmospheric extinction and can be easily derived from Table 3 (column 7). Even affecting all the quantities related to some magnitude estimate (i.e. surface brightness), this contribution does not influence the shape of the luminosity profiles and, therefore, it does not affect any estimate of the metric radius. On the contrary, the uncertainty related to the shape of the luminosity profile (including that attributable to the background removal) and to its extrapolation, affects both the magnitude and the radius. In case of luminosity profiles well represented by a generalized de Vaucouleurs law (case [b1] in Section 4.2), we estimated this contribution by examining the *r.m.s* of the $R^{1/n}$ fit as a function of n . The behaviour of this function varies with the profile. In particular, when n is large ($n > 4$), the minimum of the function $rms(n)$ is rather flat, while for small values of n it turns out to be much better defined. In any case, the best fit *r.m.s* turns out to span the range 0.02–0.04. We empirically verified that an excess of $\Delta_{rms}=0.01$ mag with respect to the minimum, always corresponds to a value of Δn which is large enough to make the new fit with $n' = n \pm \Delta n$ significantly worse than the best fit. We therefore fixed, for each galaxy, the confidence range Δn corresponding to $\Delta_{rms}=0.01$, and we derived the expected uncertainties for the total magnitude (Δm_T), metric size (ΔR) and surface brightness ($\Delta \mu$). In case of a bad fit of the luminosity profile (cases [b2] and [b3] of Section 4.2), we simply assumed the magnitude difference between the $R^{1/4}$ and exponential extrapolations to be an estimate of Δm_T , and derived the corresponding values of ΔR and $\Delta \mu$.

We illustrate in Figure 7 the adequacy of our fits to the luminosity profiles. We present the results for 3 galaxies with very different Sersic indices. The fraction of the profile actually used for the fits is indicated with the vertical, dashed lines in each panel. The best fit, obtained with the prescriptions given above, is given by the full lines. The accompanying dashed lines are for the fits corresponding to $n' = n \pm \Delta n$, n being the Sersic coefficient of the best fit. Finally, the dotted lines show the effect of the errors in the background (given in Table 6).

5.2. Ellipticity, isophotal twisting and Fourier coefficients

Apart from the global quantities extracted from the equivalent luminosity profile (n , m_T , R_{50} , $\langle \mu_{50} \rangle$, etc.), we produced some more ‘globals’ related to the geometrical profiles. In particular, we measured the ellipticity, the position angle and the Fourier coefficient c_4 (disky/boxy) of the equivalent effective isophote and at $R_{eq} = 3 \times R_{50}$. We also recorded the maximum ellipticity found on the pro-

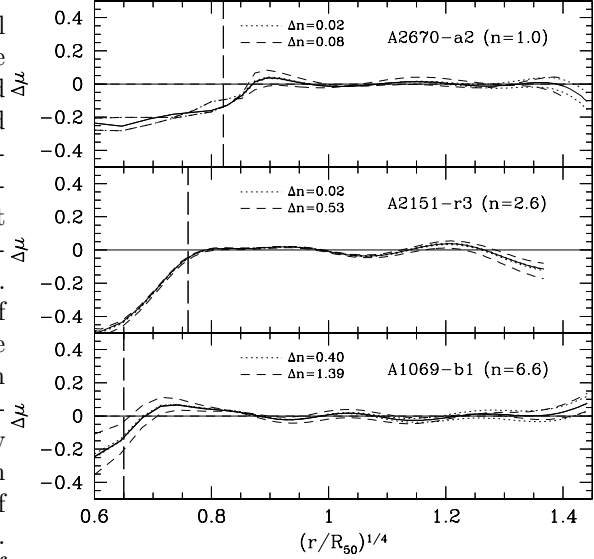


Fig. 7. Surface brightness residuals of best fitting Sersic’s law for three galaxies with very different n . The meaning of the dashed and dotted lines is explained in the text.

file (ε_{max}), the most likely value of the isophotal twisting ($\Delta\theta$), together with the minimum ($\Delta\theta_{min}$) and maximum ($\Delta\theta_{max}$) values allowed on the basis of the position angle uncertainties, and a luminosity-weighted value of c_4 (c_4^w), together with the minimum and maximum values of c_4 found on the profile (c_4^{min} , c_4^{max}). Finally, again from the luminosity profiles, we derived three different gradients of surface brightness, namely:

$$\begin{aligned}\delta\mu_1 &= (\mu_{R_{50}} - \mu_{R_{50}/2}), \\ \delta\mu_2 &= (\mu_{R_{50}/2} - \mu_{R_{50}/3}), \\ \delta\mu_3 &= (\mu_{R_{50}/4} - \mu_{R_{50}/3}).\end{aligned}$$

All the quantities relevant for our analysis are reported for each galaxy in Tables 7a,...,g. The electronic versions of these tables contain the whole information, whereas their printed versions contain only the most important entries, namely:

- Column 1:* galaxy identifier;
- Column 2:* galaxy name [NGC/IC/UGC/Dressler(1980)];
- Column 3:* morphological type;
- Column 4:* right ascension (J2000);
- Column 5:* declination (J2000);
- Column 6:* redshift (an asterisk indicates our own measurement);
- Column 7:* (m_T) total magnitude in the Gunn r band;
- Column 8:* (Δm_T) 1σ uncertainty on the total magnitude;
- Column 9:* color ($B - r$);
- Column 10:* color ($V - r$);
- Column 11:* (R_{50}) equivalent half-light radius in arcseconds, after deconvolution;
- Column 12:* (ΔR_{50}) 1σ uncertainty on the deconvolved equivalent half-light radius;

Column 13: ($\langle\mu_{50}\rangle$) mean surface brightness relative to the deconvolved half-light radius;

Column 14: ($\Delta\mu_{50}$) 1σ uncertainty on the mean surface brightness relative to the deconvolved half-light radius;

Column 15: (n) Sersic's index of the deconvolved luminosity profile;

Column 16: (Δn) 1σ uncertainty on the Sersic's index;

Column 17: (Q) quality index of the fit (good fit = 1);

Column 18: (ε_e) ellipticity of the half-light isophote;

Column 19: (ε_{max}) maximum ellipticity;

Column 20: (θ_e) position angle (clockwise from the North) of the half-light isophote;

Column 21: ($\Delta\theta$) average isophotal twisting estimated from the position angle profile;

Column 22: ($c_4(r_e)$) disk/boxy Fourier coefficient ($\times 100$) of the half-light isophote;

Column 23: (c_4^w) luminosity weighted value of the Fourier coefficient;

Column 24: ($\delta\mu_1$) surface brightness gradient ($\mu_{R_{50}} - \mu_{R_{50}/2}$);

Column 25: ($\delta\mu_2$) surface brightness gradient ($\mu_{R_{50}/2} - \mu_{R_{50}/3}$).

All the photometric and morphological parameters will be used in a forthcoming paper of the series to investigate the possibility to define some photometric version of the fundamental plane of early-type galaxies.

6. Internal and external comparisons

6.1. Check for consistency

To check the robustness of our results, we compared the surface photometry from different runs. First, we compared the different magnitudes for each standard galaxy. Table 5 lists the sample of standard galaxies we observed. For each galaxy we report the runs when it was observed, together with the average values we found for the total r magnitude, half-light radius and Sersic's index n .

In Figure 8 we report, as a function of the half-light radius in arcseconds, the differences between the individual magnitude measurements of each galaxy and the average of all available measurements for the same galaxy. Unfortunately, only for NGC 1395 observations in three different runs turned out to be available, the other standard galaxies having been observed in the same run or (at best) in two different runs. Even if this fact prevented us from performing a complete check for consistency of our photometric zero points, from Figure 8 we concluded that the uncertainties are of the order of a few hundredths of magnitude, at worst.

Then we compared the surface photometry of galaxies in our clusters. The cluster Abell 119 turned out to be the best candidate for this purpose, since it was imaged in three different observing runs (#1, #5 and #7), with three different instrumental setups (see Tables 1 and 2).

As mentioned in Section 2.3, during run #1 (DFOSC 1994) we encountered several calibration problems. The file headers were corrupted and we were able

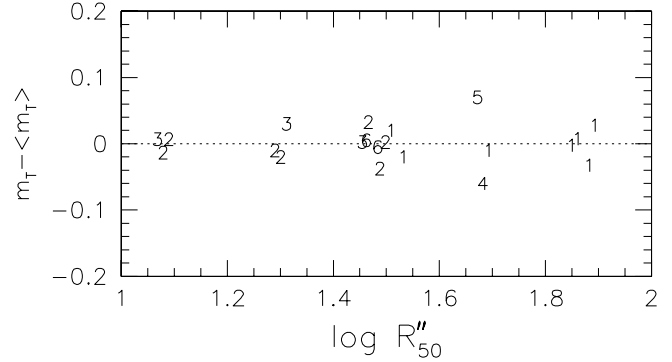


Fig. 8. Check for internal consistency for total magnitudes of standard galaxies. The numbers in the plot refer to the runs in which the standard galaxies have been observed.

to retrieve the calibration only for the night Dec. 4 (see Table 3). In spite of these problems, we tentatively decided to adopt the calibration coefficients relative to this night as representative of the whole run, checking a posteriori the possible systematic zero-point differences with the other runs. Therefore, we retrieved some exposures in the field of Abell 119 taken during the same run #1 (nights Dec. 7–8 1994) and centered on the galaxies *D41*, *D99* and *D105* (our identifications: *b5*, *e1* and *g4*, respectively). We also retrieved an exposure taken during run #5, centered on the galaxy *D105*.

In summary, we compared imaging from the three runs #1, #5 and #7, for the above mentioned fields. In each field more than 15 galaxies of various sizes and luminosity turned out to be in common among the different runs. Again the *AIAP* tool was used to analyze the galaxies in the retrieved frames, providing their luminosity and geometrical profiles, as well as their global parameters.

In Figure 9 the differences between different kinds of magnitudes derived for each galaxy from different runs are shown. In particular, in the lower panels we illustrate the magnitude differences relative to the isophote $\mu_r = 24$. Being insensitive to the adopted extrapolation of the luminosity profiles (see Section 4.2), these differences should give indication about the true biases affecting the different runs. As expected, the calibration relative to run #1 turned out to be inaccurate. In particular, accordingly to Figure 9, a systematic zero point correction of ~ 0.1 mag was applied to the magnitudes of galaxies observed during that run. In the upper and middle panels we report the magnitude differences obtained by using the pure $R^{1/4}$ ($n=4$) and exponential ($n=1$) extrapolations (depurated from the previous biases), respectively. They give an indication of the maximum uncertainties inherent to the extrapolation procedure.

The binned and averaged residuals of ellipticity, position angle and Fourier coefficient for the galaxies in common among the three runs, are plotted in Figure 10 as a function of the isophotal semi-major axis. Figure 10 shows

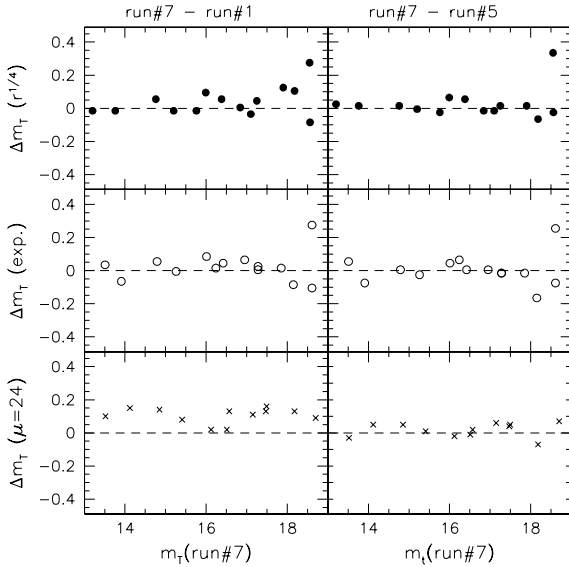
Table 5. The sample of standard galaxies

Name	Type	$\alpha(2000)$			$\delta(2000)$			runs	$r_T^{(1)}$	$R_{50}^{(2)''}$	$n^{(3)}$
NGC 1199	<i>E3</i>	03 ^h	03 ^m	38. ^s 6	-15°	36'	51''	4	11.38	25.5	5.5 ± 0.07
NGC 1395	<i>E2</i>	03	38	29.6	-23	01	40	1, 4, 5	9.89	48.1	5.0 ± 0.04
NGC 1407	<i>E0</i>	03	40	11.8	-18	34	48	1	9.70	74.4	6.6 ± 0.12
NGC 1439	<i>E1</i>	03	44	49.9	-21	55	13	1	11.18	33.2	9.7 ± 0.08
NGC 1726	<i>S0</i>	04	59	41.8	-07	45	16	6	11.19	29.7	3.2 ± 0.06
NGC 2340	<i>E</i>	07	11	10.8	+50	10	28	6	11.34	51.0	3.1 ± 0.03
NGC 2986	<i>E2</i>	09	44	16.0	-21	16	41	5	10.51	41.0	9.5 ± 0.09
NGC 4839	<i>S0</i>	12	57	24.2	+27	29	54	2	11.88	37.4	2.9 ± 0.11
NGC 4841A	<i>E</i>	12	57	32.0	+28	28	38	2, 3	12.20	20.0	6.8 ± 0.14
NGC 4841B	<i>E</i>	12	57	33.9	+28	28	54	2, 3	13.11	12.0	4.6 ± 0.04
NGC 4874	<i>E</i>	12	59	35.9	+27	57	31	2	11.07	77.5	3.5 ± 0.06
NGC 4889	<i>E4</i>	13	00	07.7	+27	58	33	2, 3	11.03	30.0	5.5 ± 0.13

(1) average total apparent magnitude in the Gunn *r* band

(2) average half light radius in arcseconds

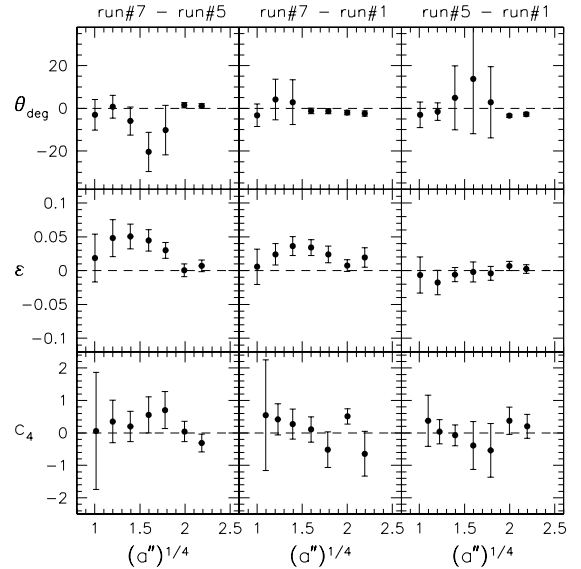
(3) best fit Sersic's index and relative uncertainty

**Fig. 9.** Check for internal consistency for different kinds of magnitudes.

a general good agreement among the morphological profiles of the same galaxies obtained in different runs. The wave-like behaviour of the ellipticity residuals in the comparisons involving run #7 can be easily explained by the better seeing of this run, which is likely to produce a better representation of the inner (possibly flat) isophotes.

6.2. External comparisons

We compared our photometry with the data available in the literature for the nearby standard galaxies we observed during the various runs (see Table 5). In partic-

**Fig. 10.** Binned and averaged differences in the ε , θ and c_4 profiles of galaxies in Abell 119 from the comparison of different observing runs in pairs.

ular, in Figure 11 our photometry is compared with that of Jørgensen and Franx (1994) and Jørgensen et al. (1995; both indicated by JFK in the plots), as well as with the data collection from Paturel et al. (1997; LEDA) and with the results given by Faber et al. (1987, FA+ in the plots). Our observations in the *r* band were directly compared with the corresponding ones from JFK, whereas, to compare with the magnitudes from LEDA and FA+, we have converted them into the *r* band by using our colors ($B-r$). We found:

$$\langle m_T(\text{our}) - m_T(\text{other}) \rangle = 0.005 \pm 0.025 \text{ mag (r.m.s.} = 0.112),$$

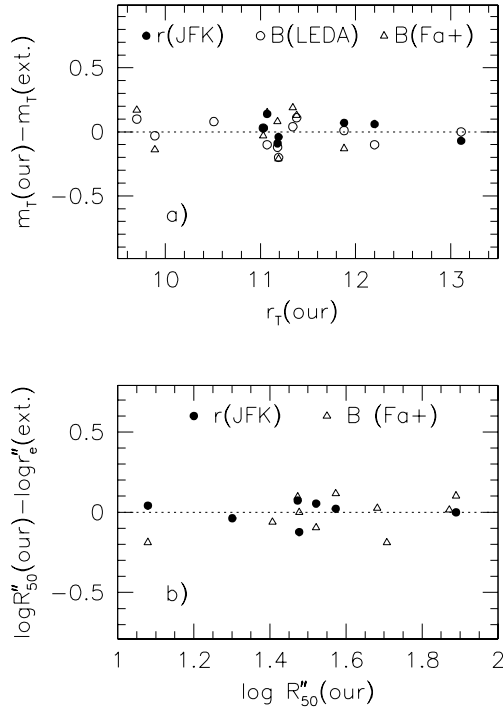


Fig. 11. Total magnitudes and effective radii of nearby standard galaxies from our surface photometry are compared with the values given by JF and JFK (full dots), by Paturel et al. (1997; open dots) and by Faber et al. (1987; open triangles).

$$\langle \log R_{50}(\text{our}) - \log R_e(\text{other}) \rangle = 0.009 \pm 0.023 \text{ (r.m.s.} = 0.095).$$

It is worth stressing that the methodologies used in the above mentioned works to derive total magnitudes and effective radii differ from ours and also differ from each one another. In particular, our R_{50} is defined as the equivalent radius enclosing half of the total galaxy light (irrespective of the shape of the luminosity profile), while past work generally derive the effective radius R_e assuming an $r^{1/4}$ profile. This produces systematically different results, depending on the true luminosity profile shape, and likely explains the relatively large scatter we find in comparing the radius estimates (22%). Actually, an even larger scatter (30%) was suggested to be expected by Kelson et al. (2000) in their extensive discussion of comparisons of R_{50} derived from bulge+disk fits and from Sersic's law fits.

7. Summary and future plans

This paper mainly deals with the illustration of the photometric data we have collected in the framework of a long term project aimed at investigating systematically the so called 'scaling relations' of early-type galaxies in clusters. The main goal of this project is to throw light upon the

cosmic variance of the scaling relations themselves, as well as upon their possible dependence on the redshift.

We start here discussing the reduction and calibration procedures we have applied to the whole photometric data set, relative to the global sample of 22 clusters in different bins of redshift, up to $z \sim 0.25$. Then, we present the detailed surface photometry of 312 early-type galaxies in 7 nearby clusters belonging to the first redshift bin and defining the local reference sample. The whole set of luminosity and geometrical profiles is placed at reader's disposal (in both tabular and postscript format) in the electronic version of the paper, while several global photometric and structural parameters are evaluated for each galaxy and are collected in tables (one for each cluster), which again are at reader's disposal.

Here we do not try to analyze the data in the tables, nor to seek for possible correlations among the various parameters. These items will be addressed in the third paper of this series, where the scaling relations of early-type galaxies in the local sample of clusters will be discussed in detail, using both the photometric and the spectroscopic information. We will present the latter one in the second (forthcoming) paper of this series, where the results of both the low- and the intermediate- resolution spectroscopy for a subsample of the present galaxy sample will be discussed.

The two final steps of the series will concern the detailed surface photometry of early-type galaxies in the remaining 15 (more distant) clusters and the analysis of the scaling relations as a function of different parameters, including the redshift of the cluster.

References

- Abell G.O., Corwin H.G.Jr., Olowin R.P., 1989, ApJS 70, 1
- Bautz L.P., Morgan W.W., 1970, ApJ 162, L149
- Bender R., Burstein D., Faber S., 1992, ApJ 399, 462
- Bender R., Saglia R.P., Ziegler B., Belloni P., Greggio L., Hopp U., Bruzual G., 1998, ApJ, 493, 529
- Bendinelli O., 1991, ApJ 366, 599
- Bertin E., Arnouts S., 1996, A&AS 117, 393
- Caon N., Capaccioli M., D'Onofrio M., 1993, MNRAS 265, 1013
- Capaccioli M., Caon N., D'Onofrio M., 1992, MNRAS 259, 323
- Ciotti L., 1991, A&A 249, 99
- Ciotti L., Lanzoni B., Renzini A., 1996, MNRAS 282, 1
- Djorgovski S., Davis M., 1987, ApJ 313, 59
- van Dokkum P.G., Franx M., 1996, MNRAS 281, 985
- Dressler A., 1980, ApJ 236, 351
- Dressler A., Lynden-Bell D., Burstein D., Davies R.L., Faber S.M., Terlevich R., Wegner G., 1987, ApJ 313, 42
- Dressler A., Oemler, A.Jr., Couch, W.J., Smail, I., Ellis, R.S., Barger, A., Butcher, H., Poggianti, B.M., Sharples, R.M., 1997, ApJ 490, 577
- Faber S.M., Dressler A., Davies R.L., Burstein D., Lynden-Bell D., 1987, in: Proc of Santa Cruz Summer Workshop in Astronomy and Astrophysics, p.175. Springer-Verlag edition
- Fasano G., 1990, Internal report of the Padova Astronomical Observatory

- Fasano G., Bonoli, C., 1990, A&A 234, 89
- Fasano G., Falomo R., Scarpa R., 1996, MNRAS 282, 40
- Fasano G., Bettoni D., Kjærgaard P., Moles M., 1997, *Galaxy Scaling Relations: Origins, Evolution and Applications*, proceedings from the ESO Workshop held November, 1996, edited by Luiz Nicolaci da Costa and Alvio Renzini (Springer-Verlag), p. 344.
- Fasano G., Cristiani S., Arnouts S., Filippi M., 1998, AJ 115, 1400
- Fasano G., Filippi M., 1998, A&AS 129, 583
- Fasano G., Poggianti B.M., Couch W.J., Bettoni D., Kjærgaard P., Moles M., 2000, ApJ 542, 673
- Franceschini A., Silva L., Fasano G., Granato L., Bressan A., Arnouts S., Danese L., 1998, ApJ 506, 600
- Gladders M.D., López-Cruz O., Yee H.K.C., Kodama T., 1998, ApJ 501, 571
- Graham A., Lauer T.R., Colless M., Postman M., 1996, ApJ 465, 534
- Guzman R., Lucey J.R., Bower R.G., 1993, MNRAS 265, 731
- Jørgensen I., 1994, PASP 106, 967
- Jørgensen I., 1999, MNRAS 306, 607
- Jørgensen I., 2000, PASP 106, 967
- Jørgensen I., Franx M., 1994, ApJ 433, 553
- Jørgensen I., Franx M., Kjærgaard P., 1995, MNRAS 273, 1097
- Jørgensen I., Franx M., Kjærgaard P., 1996, MNRAS 280, 167
- Jørgensen, Hjorth, J., 1997, *Galaxy Scaling Relations: Origins, Evolution and Applications*, proceedings from the ESO Workshop held November, 1996, edited by Luiz Nicolaci da Costa and Alvio Renzini (Springer-Verlag), p. 175.
- Jørgensen, I., Franx, M., Hjorth, J., van Dokkum, P.G., 1999, MNRAS 280, 167
- Kelson D.D., van Dokkum P.G., Franx M., Illingworth G.D., Fabricant D., 1997, ApJ 478, L13
- Kelson D.D., Illingworth G.D., van Dokkum P.G., Franx M., 2000, ApJ 531, 184
- Kjærgaard P., Jørgensen I., Moles M., 1993, ApJ 418, 617 (KJM)
- Landolt A.U., 1992, AJ 104, 340
- Metcalfe N., Shanks T., Fong R., Roche N., 1995, MNRAS 273, 257
- Mobasher B., Guzmán R., Aragón-Salamanca A., Zepf S., 1999, MNRAS 304, 225
- Moles M., Campos A., Kjærgaard P., Fasano G., Bettoni D., 1998, ApJ 495, L31
- Moles M., Bettoni D., Kjærgaard P., Fasano G., 2001, in preparation
- Montgomery, K.A., Marschall, L.A., Janes, K.A., 1993, AJ 106,181
- Pahre M.A., Djorgovski S.G., 1995, ApJ 449, L1
- Pahre M.A., Djorgovski S.G., de Carvalho R.R., 1996, ApJ 456, L79
- Pahre M.A., Djorgovski S.G., de Carvalho R.R., 1998, AJ 116, 1591
- Paturel G., Andernach H., Bottinelli L., di Nella H., Durand N., Garnier R., Gouguenheim L., Lanoix P., Marthinet M.C., Petit C., Rousseau J., Theureau G., Vauglin I., 1997, A&AS 124, 109
- Peletier R.F., Davies R.L., Illingworth G.D., Davis L.E., Cawson M., 1990, AJ 100, 1091
- Pierini D., Gavazzi G., Franzetti P., Scodreggio M., Boselli A., 2000, *The Extragalactic Infrared Background and its Cosmological Implications*, IAU Symp.no. 204. Manchester, England, August 2000.
- Pignatelli E., Fasano G., 1999, Ap&SS 269, 657
- Rood H.J., Sastry, G.N., 1971, PASP 83, 313
- Schlegel D.J., Finkbeiner D.P., Davis M., 1998, ApJ 500, 525
- Sersic J.L., 1968, *Atlas de galaxias australes*, Cordoba, Argentina: Observatorio Astronomico
- Yee H.K.C., Gladders M.D., López-Cruz O., 1999, *Photometric Redshifts and the Detection of High Redshift Galaxies*, ASP Conference Series, Vol.191, Edited by WeymannR., Storrie-Lombardi L., Sawicki M., Brunner R., p.166
- Ziegler B.L., Saglia R.P., Bender R., Belloni P., Greggio L., Seitz S., 1999, A&A, 346, 13

Acknowledgements. We wish to thank the referee Dan Kelson for the very useful suggestions which helped us to greatly improve the final version of the paper.

Table 6. The observed fields

Cluster	Field	Run	α_c	δ_c	$FWHM$	Background ⁽¹⁾	$N_{gal}^{(2)}$
			(2000)	(2000)	"	rel.err.	
A 2151	a	2	16 : 02 : 48.8	17 : 09 : 59	0.6	0.005	2
	b	2	16 : 04 : 19.1	17 : 10 : 48	0.7	0.008	1
	c	3	16 : 03 : 31.8	17 : 11 : 53	0.7	0.005	1
	d	2	16 : 04 : 02.3	17 : 16 : 52	0.7	0.005	1
	e	2	16 : 05 : 32.6	17 : 35 : 54	0.7	0.005	1
	f	2	16 : 04 : 38.0	17 : 42 : 44	0.5	0.005	1
	g	2	16 : 04 : 33.2	17 : 43 : 15	0.9	0.010	7
	h	2	16 : 05 : 08.7	17 : 43 : 47	0.5	0.010	2
	i	2	16 : 03 : 18.0	17 : 43 : 56	0.8	0.005	1
	j	2	16 : 06 : 38.9	17 : 45 : 37	0.6	0.005	2
	k	2	16 : 05 : 38.5	17 : 46 : 02	0.5	0.010	1
	l	2	16 : 05 : 01.2	17 : 46 : 29	0.4	0.005	2
	m	2	16 : 06 : 47.6	17 : 47 : 20	0.6	0.005	1
	n	2	16 : 05 : 36.5	17 : 48 : 04	0.4	0.005	2
	o	2	16 : 04 : 59.4	17 : 52 : 10	0.6	0.005	1
	p	2	16 : 05 : 40.3	18 : 06 : 22	0.8	0.005	2
	q	2	16 : 05 : 39.6	18 : 09 : 52	0.7	0.005	1
r	2	16 : 06 : 16.1	18 : 14 : 58	0.6	0.010	3	
A 119	a	5	00 : 56 : 54.6	-01 : 16 : 36	1.7	0.010	8
	b	7	00 : 56 : 53.0	-01 : 16 : 28	1.0	0.005	9
	c	1	00 : 56 : 19.9	-01 : 13 : 46	1.5	0.005	18
	d	7	00 : 57 : 15.4	-01 : 00 : 50	0.8	0.005	4
	e	7	00 : 55 : 55.9	-00 : 55 : 17	0.9	0.005	2
	f	5	00 : 55 : 59.5	-00 : 54 : 19	1.7	0.010	7
	g	7	00 : 56 : 58.8	-00 : 52 : 06	0.9	0.005	6
A 1983	a	3	14 : 54 : 39.5	16 : 13 : 11	0.7	0.008	1
	b	3	14 : 54 : 22.5	16 : 21 : 02	0.7	0.009	4
	c	3	14 : 54 : 10.6	16 : 26 : 02	0.7	0.005	1
	d	3	14 : 51 : 16.4	16 : 25 : 55	0.7	0.005	1
	e	3	14 : 55 : 28.0	16 : 27 : 23	0.6	0.005	1
	f	3	14 : 54 : 05.9	16 : 31 : 31	0.6	0.005	1
	g	3	14 : 53 : 07.2	16 : 35 : 16	1.1	0.005	1
	h	3	14 : 52 : 57.4	16 : 41 : 35	1.3	0.006	7
	i	3	14 : 52 : 54.5	16 : 41 : 58	0.6	0.006	1
	j	3	14 : 52 : 45.5	16 : 42 : 50	0.8	0.005	4
	k	3	14 : 49 : 56.4	16 : 48 : 29	0.7	0.050	2
	l	3	14 : 52 : 24.3	16 : 50 : 44	0.7	0.010	1
	m	3	14 : 52 : 42.6	16 : 54 : 02	1.0	0.020	1
	n	3	14 : 54 : 14.9	16 : 54 : 41	0.7	0.010	1
	o	3	14 : 53 : 08.9	17 : 02 : 26	0.7	0.010	1
	p	3	14 : 52 : 22.8	17 : 07 : 07	0.9	0.008	1
	q	3	14 : 52 : 13.1	17 : 14 : 47	1.1	0.006	2

⁽¹⁾ see text⁽²⁾ number of selected galaxies in the field

....Continue....

Table 6. The observed fields (Continue..)

Cluster	Field	Run	α_c (2000)	δ_c (2000)	$FWHM$ "	Background rel.err.	N_{gal}
DC 2103	a	4	21 : 08 : 59.6	-39 : 51 : 04	1.1	0.002	9
	b	4	21 : 06 : 04.5	-39 : 35 : 42	1.2	0.003	17
	c	4	21 : 07 : 47.6	-39 : 29 : 08	1.2	0.004	15
A 3125	a	5	03 : 26 : 43.3	-53 : 50 : 03	1.2	0.008	2
	b	5	03 : 29 : 12.8	-53 : 28 : 36	1.5	0.002	5
	c	5	03 : 27 : 43.5	-53 : 23 : 34	1.0	0.003	16
	d	5	03 : 23 : 55.0	-53 : 18 : 29	1.3	0.005	11
	e	5	03 : 27 : 01.7	-53 : 08 : 36	1.6	0.001	6
	f	5	03 : 24 : 11.6	-53 : 08 : 28	1.2	0.001	11
	g	5	03 : 23 : 16.4	-53 : 05 : 28	1.4	0.002	5
	h	5	03 : 30 : 53.7	-52 : 51 : 05	1.3	0.001	11
	i	5	03 : 28 : 02.1	-52 : 40 : 28	1.4	0.002	4
A 1069	a	5	10 : 37 : 37.4	-09 : 09 : 08	1.5	0.012	5
	b	5	10 : 40 : 38.3	-08 : 51 : 27	1.3	0.004	2
	c	5	10 : 39 : 47.0	-08 : 37 : 44	1.6	0.004	8
	d	5	10 : 40 : 05.2	-08 : 22 : 05	1.2	0.004	4
	e	5	10 : 41 : 57.8	-08 : 12 : 42	1.6	0.006	10
	f	5	10 : 38 : 19.3	-08 : 11 : 42	1.4	0.004	12
	g	5	10 : 40 : 41.2	-07 : 58 : 17	1.4	0.006	9
A 2670	a	7	23 : 54 : 16.0	-10 : 25 : 10	1.1	0.002	33

Table 7. a – Photometric and morphological parameters of galaxies in Abell 2151

Galaxy	Name	Type	$\alpha(2000)$	$\delta(2000)$	z	m_T	Δm	$(B-r)$	$(V-r)$	R_{50}	ΔR_{50}	$\langle\mu_{50}\rangle$	$\Delta\mu_{50}$	n	Δn	Q	ε_e	ε_{max}	θ_e	$\Delta\theta$	$c_4(r_e)$	c_4^w	$\delta\mu_1$	$\delta\mu_2$
a1	D9	E/SO	16 02 49.1	17 10 05	0.0347	14.81	0.03	1.37		4.29	0.20	19.95	0.06	2.80	0.14	0	0.28	0.41	142.5	24.3	0.66	0.29	1.11	0.60
a2		SO	16 02 47.3	17 10 56		17.07	0.02	1.31		2.58	0.06	21.07	0.06	0.90	0.26	1	0.36	0.48	16.2	7.1	1.28	0.26	1.14	0.58
b1	D4	E	16 04 19.5	17 10 49	0.0341	14.62	0.02	1.24		4.64	0.18	19.97	0.06	3.10	0.47	1	0.07	0.19	158.2	63.6	-0.27	-0.23	1.24	0.58
c1	N6034	E	16 03 32.0	17 11 55	0.0339	13.23	0.12	1.44		14.63	4.21	21.04	0.38	11.60	4.58	1	0.22	0.26	120.9	18.2	-0.63	-0.52	1.24	0.76
d1	D15	E/SO	16 04 02.7	17 16 56	0.0330	14.49	0.02	1.42		4.91	0.16	19.89	0.05	4.50	0.40	1	0.27	0.38	136.6	3.4	-0.17	0.06	1.22	0.60
e1	I1178	E	16 05 33.1	17 36 05	0.0337	13.74	0.05	1.40		6.33	0.59	19.74	0.15	3.00	1.61	1	0.14	0.18	101.8	86.9	0.60	-0.55	1.29	0.67
f1	N6042	E	16 04 39.6	17 42 02	0.0357	13.57	0.03	1.40		15.39	0.74	21.53	0.07	4.30	0.56	1	0.17	0.21	129.9	11.0	0.05	0.05	1.23	0.68
g1		E	16 04 35.0	17 42 49		16.12	0.02	1.43		0.70	0.02	17.40	0.17	3.30	3.13	0	0.15	0.23	174.2	14.8	0.70	1.26	1.77	0.51
g2	D65	SO	16 04 35.1	17 43 10	0.0376	15.16	0.02	1.32		3.03	0.13	19.51	0.06	5.40	0.47	1	0.19	0.29	119.3	13.7			1.23	0.75
g3	N6041	E	16 04 35.8	17 43 16	0.0348	13.06	0.02	1.38		30.27	0.94	22.05	0.04	7.40	0.41	1	0.23	0.25	125.3	22.5	1.53	0.84	1.23	0.61
g4	I1170	SO/E	16 04 31.8	17 43 17	0.0320	14.96	0.02	1.37		3.87	0.12	19.85	0.06	1.40	0.33	1	0.44	0.52	92.3	2.7	1.59	0.73	1.18	0.61
g5		E/SO	16 04 35.1	17 43 47		16.76	0.02	1.27		1.61	0.06	19.76	0.09	6.20	2.91	1	0.05	0.26	158.7	19.7	0.12	0.15	1.27	0.74
g6		E	16 04 32.4	17 44 10		17.29	0.03	1.31		0.68	0.02	18.53	0.11	2.10	1.32	0	0.12	0.18	120.9	35.6	-1.04	-0.15	1.10	0.23
g7		E	16 04 38.2	17 44 32		18.47	0.04	1.34		0.59	0.02	19.40	0.11	1.50	0.92	0	0.09	0.12	116.1	89.8	-0.48	0.25	0.84	0.16
h1	D98	E	16 05 10.2	17 43 06		16.80	0.02	1.31		1.01	0.04	18.85	0.13	4.10	2.90	1	0.02	0.08	2.8	43.3	1.11	0.17	1.69	0.71
h2	N6047	E	16 05 09.0	17 43 49	0.0312	13.32	0.05	1.39		22.44	2.26	21.88	0.14	5.70	1.15	1	0.17	0.29	51.1	51.4	-3.53	-1.91	1.50	0.64
i1	D69	E	16 03 18.2	17 43 57	0.0350	15.13	0.03	1.25		4.84	0.32	20.43	0.09	5.70	0.81	1	0.11	0.23	165.6	90.1	-0.27	0.09	1.36	0.67
j1	I1194	E	16 06 39.3	17 45 40	0.0390	14.04	0.03	1.43		3.99	0.18	19.06	0.06	4.80	0.58	1	0.05	0.32	167.2	51.2	0.59	-0.10	1.23	0.71
j2	D73	SO	16 06 38.8	17 47 01	0.0373	15.29	0.05	1.39		4.94	0.31	20.65	0.11	1.60	0.64	0	0.32	0.33	158.4	42.3	0.02	0.86	1.01	0.56
k1	I1183	E/SO	16 05 38.2	17 46 00	0.0335	14.17	0.04	1.43		6.45	0.45	20.15	0.09	10.20	1.01	1	0.24	0.43	117.4	36.6	0.48	0.57	1.21	0.66
l1		Sa/0	16 05 01.0	17 46 23		16.75	0.05	1.26		1.59	0.10	19.75	0.11	1.50	0.69	1	0.53	0.61	151.9	5.9	1.90	0.06	1.22	0.56
l2	N6043	E	16 05 01.5	17 46 30	0.0334	14.09	0.03	1.38		6.50	0.29	20.14	0.06	3.70	0.49	1	0.29	0.32	113.1	52.6	0.29	0.06	1.23	0.68
m1	D71	E	16 06 47.9	17 47 23	0.0419	16.03	0.02	1.22		2.15	0.06	19.69	0.04	2.30	0.27	1	0.18	0.19	127.3	6.0	-0.17	-0.37	1.18	0.63
n1	I1182	Ep	16 05 36.8	17 48 08	0.0342	13.99	0.03	1.42		7.32	0.31	20.33	0.06	3.90	0.46	1	0.20	0.23	116.7	36.9	1.24	-0.60	1.24	0.59
n2		SO	16 05 32.2	17 48 31		17.97	0.00	1.13		0.91	0.00	19.78	0.01	0.70	0.06	0	0.48	0.58	22.6	4.6	2.02	2.14	1.38	0.63
o1	N6044	E	16 04 59.8	17 52 12	0.0331	14.12	0.01	1.21		5.25	0.11	19.73	0.03	2.40	0.22	1	0.07	0.08	62.7	88.3	0.24	-0.10	1.15	0.58
p1	D157	E	16 05 40.8	18 06 26	0.0379	14.89	0.04	1.29		4.76	0.44	20.28	0.13	5.40	1.46	1	0.14	0.19	117.7	10.0	0.07	-0.35	1.31	0.82
p2		SO	16 05 41.6	18 06 52		17.45	0.02	1.44		1.85	0.05	20.73	0.09	1.20	0.64	1	0.39	0.43	42.3	5.4	2.13	0.83	1.36	0.77
q1	N6053	E	16 05 39.6	18 09 51	0.0353	14.33	0.03	1.35		6.23	0.26	20.34	0.06	4.10	0.54	1	0.07	0.09	55.1	46.2	-0.90	-0.48	1.19	0.64
r1		E/SO	16 06 14.5	18 14 55		17.35	0.05	1.26		3.18	0.24	21.72	0.18	1.60	1.44	1	0.37	0.37	104.7	3.8	1.05	-0.21	1.21	0.65
r2	N6061	E	16 06 16.0	18 15 00	0.0368	13.06	0.01	1.37		15.02	0.38	21.01	0.03	4.90	0.31	1	0.21	0.22	91.0	4.2	-0.29	-0.22	1.21	0.64
r3		E	16 06 17.7	18 15 11		17.55	0.03	1.24		1.43	0.05	20.32	0.06	2.30	0.53	1	0.26	0.28	150.1	11.0	-1.35	-1.01	0.92	0.50

Table 7. b – Photometric and morphological parameters of galaxies in Abell 119

Galaxy	Name	Type	$\alpha(2000)$	$\delta(2000)$	z	m_T	Δm	$(B-r)$	$(V-r)$	R_{50}	ΔR_{50}	$\langle \mu_{50} \rangle$	$\Delta \mu_{50}$	n	Δn	Q	ε_e	ε_{max}	θ_e	$\Delta \theta$	$c_4(r_e)$	c_4^w	$\delta \mu_1$	$\delta \mu_2$
a1	D33	E	00 56 31.5	-01 21 41	0.0418	16.18	0.07		0.41	4.03	0.58	20.83	0.20	10.00	4.46	1	0.05	0.18	32.6	66.8	0.23	0.04	1.40	0.76
a2	D32	SO/E	00 56 38.5	-01 21 07		16.76	0.03		0.28	1.26	0.06	19.06	0.07	3.30	0.58	1	0.15	0.45	47.1	6.5		2.29	1.48	0.41
a3		Sa/0	00 57 02.9	-01 20 41		17.49	0.02		0.18	2.60	0.06	21.33	0.03	1.90	0.20	1	0.48	0.54	123.7	8.9	2.08	-0.3	1.06	0.55
a4		Sa/0	00 56 37.7	-01 20 41		18.27	0.03		0.29	1.45	0.04	20.84	0.05	1.00	0.27	1	0.35	0.49	38.6	2.3	-0.19	2.08	0.90	0.18
a5		dE	00 57 05.4	-01 19 20		18.68	0.08		0.13	1.00	0.07	20.65	0.19	1.40	2.79	0	0.07	0.10	83.0	62.4		-0.02	0.93	0.18
a6		E/S0	00 57 10.5	-01 17 30		18.04	0.01		0.21	1.94	0.03	21.29	0.03	1.00	0.13	1	0.18	0.27	112.3	4.8	-0.97	-0.21	1.14	0.39
a7	D40	SB0	00 57 14.6	-01 17 09	0.0428	15.52	0.03		0.24	4.87	0.20	20.65	0.08	1.60	0.58	0	0.39	0.46	161.6	12.4	3.53	0.50	1.00	0.39
a8		SO/E	00 56 35.7	-01 15 56	0.0440	16.86	0.03		0.30	3.32	0.13	21.14	0.06	2.10	0.46	1	0.37	0.39	73.0	7.1	1.67	0.35	1.05	0.69
b1		E/S0	00 56 41.0	-01 18 26		17.42	0.02	1.10		0.84	0.03	19.07	0.05	1.90	0.30	1	0.24	0.34	17.8	13.4	-0.20	0.87	1.51	0.57
b2		SO/E	00 56 45.1	-01 18 01		17.27	0.03	1.09		2.25	0.08	20.99	0.06	1.70	0.39	1	0.46	0.51	13.5	5.2	1.26	0.48	1.16	0.55
b3		E	00 56 53.2	-01 17 41		18.37	0.03	0.99		1.54	0.07	21.33	0.07	2.60	0.52	1	0.19	0.25	70.9	15.7	-0.20	-0.61	1.32	0.72
b4		Ep	00 56 49.1	-01 17 32		17.37	0.02	1.23		1.60	0.03	20.40	0.03	0.90	0.12	0	0.05	0.18	86.4	65.9	0.85	1.76	0.84	0.68
b5	D41	S0	00 56 51.5	-01 16 20	0.0407	14.78	0.02	1.19		2.86	0.06	19.05	0.03	1.50	0.18	1	0.49	0.75	90.0	1.2	10.52	7.12	0.96	0.51
b6		Sa/0	00 56 59.7	-01 15 54		17.94	0.02	1.08		1.93	0.04	21.32	0.03	1.20	0.15	0	0.57	0.69	75.1	1.9	3.91	2.05	0.95	0.51
b7	D57	E	00 56 58.5	-01 15 25		16.37	0.02	1.21		2.29	0.06	20.21	0.04	1.50	0.22	1	0.03	0.21	113.7	190.1	1.02	0.56	1.06	0.60
b8		E/S0	00 56 56.1	-01 14 46		18.25	0.01	1.23		1.19	0.01	20.64	0.02	1.00	0.08	0	0.20	0.24	90.0	15.2	0.63	0.38	0.87	0.55
b9		E/S0	00 56 42.8	-01 13 24		18.66	0.03	1.00		1.24	0.05	21.18	0.06	3.70	0.62	1	0.33	0.39	26.6	7.5	2.33	0.37	1.43	0.54
c1		E	00 56 17.7	-01 17 43		17.73	0.03		0.31	1.49	0.06	20.32	0.05	3.30	0.39	1	0.15	0.23	54.8	12.5		-0.49	1.38	0.65
c2		E	00 56 24.7	-01 16 40		16.53	0.07		0.35	8.34	0.86	22.82	0.15	5.00	2.15	1	0.08	0.28	102.6	14.0	7.13	0.34	1.32	0.65
c3	D44	E	00 56 25.9	-01 16 28	0.0428	14.76	0.03		0.40	5.69	0.30	20.18	0.08	9.40	1.89	1	0.02	0.08	83.0	22.1	0.52	-0.46	1.40	0.72
c4	D46	E	00 56 13.1	-01 16 11	0.0452	16.09	0.05		0.34	1.46	0.12	18.67	0.18	1.70	1.50	0	0.06	0.14	118.0	48.8		0.22	1.69	0.47
c5	D67	E	00 56 10.2	-01 16 03	0.0455	16.39	0.03		0.31	1.40	0.05	18.91	0.05	2.10	0.30	1	0.10	0.25	69.3	18.4		0.34	1.22	0.63
c6	U 583	E	00 56 25.6	-01 15 46	0.0382	13.52	0.03		0.32	13.49	0.86	20.86	0.09	5.30	0.88	1	0.15	0.16	58.2	31.5	0.23	-0.07	1.36	0.73
c7		S0	00 56 15.0	-01 15 46		17.32	0.02		0.32	2.42	0.07	20.86	0.05	2.10	0.33	1	0.46	0.52	77.2	2.4	2.62	0.40	1.19	0.61
c8	U 579	E	00 56 16.1	-01 15 19	0.0444	12.44	0.05		0.32	70.63	5.95	23.20	0.12	8.50	1.90	1	0.34	0.37	144.7	12.0	6.26	1.00	1.30	0.66
c9		SO/a	00 56 20.4	-01 15 03		18.36	0.04		0.10	1.29	0.07	20.93	0.08	1.60	0.40	1	0.27	0.35	68.8	4.3		0.30	1.42	0.43
c10		E	00 56 20.3	-01 14 33		17.29	0.04		0.18	0.96	0.07	19.12	0.10	2.30	0.67	1	0.13	0.16	26.3	8.8		0.06	1.61	0.65
c11	D62	E	00 56 18.1	-01 14 31	0.0435	15.44	0.05		0.15	2.01	0.16	18.86	0.14	2.40	1.43	0	0.02	0.07	31.4	42.2	-0.17	-0.06	1.50	0.71
c12		Sa/0	00 56 13.4	-01 14 18	0.0484	17.08	0.02		0.12	2.68	0.07	21.15	0.04	3.90	0.30	1	0.29	0.37	48.1	5.4	0.83	-0.25	1.25	0.51
c13		E	00 56 25.3	-01 13 50		18.19	0.01		0.15	1.11	0.02	20.33	0.06	6.50	2.10	0	0.11	0.19	1.7	21.7		-0.43	2.18	0.53
c14	D61	SB0	00 56 22.9	-01 12 34	0.0498	14.11	0.03		0.28	5.50	0.20	19.58	0.06	1.80	0.42	0	0.41	0.47	67.8	12.5	0.72	0.93	0.98	0.64
c15		SO/a	00 56 08.6	-01 11 59		17.97	0.02		0.32	0.98	0.02	19.73	0.05	6.20	1.61	0	0.14	0.26	157.9	3.8		1.36	0.90	0.17
c16		dE	00 56 28.4	-01 11 41		18.41	0.00		0.16	1.85	0.01	21.74	0.15	1.20	1.10	0	0.10	0.19	103.5	25.6		-1.63	1.46	1.00
c17	D75	E/S0	00 56 21.0	-01 10 35	0.0429	15.11	0.02		0.31	3.91	0.11	19.76	0.05	1.80	0.31	1	0.37	0.51	150.3	2.7	1.11	0.70	1.06	0.51
c18	D74	E/S0	00 56 30.7	-01 10 22	0.0457	15.47	0.04		0.29	3.15	0.19	19.72	0.09	5.20	1.11	1	0.27	0.37	177.3	8.9	2.09	1.27	1.24	0.84
d1		S0p	00 57 16.0	-01 01 58		18.06	0.05	1.36		1.85	0.12	21.42	0.09	3.20	0.61	0	0.46	0.60	77.8	5.6	4.84	4.98	0.78	0.81
d2	D94	E/S0	00 57 10.7	-01 01 07	0.0419	15.38	0.08	1.24		3.11	0.50	19.86	0.22	10.00	4.09	0	0.39	0.44	122.3	4.4	0.83	0.15	1.39	0.63
d3	D93	E/S0	00 57 13.7	-01 00 43	0.0435	15.01	0.04	1.28		2.55	0.16	19.07	0.10	2.50	0.92	1	0.28	0.35	135.5	12.3	0.89	0.63	1.17	0.61
d4		dE	00 57 13.5	-01 00 39		18.69	0.04	1.11		0.85	0.05	20.38	0.09	1.10	0.39	0	0.14	0.15	178.7	25.9	0.70	-0.26	1.50	0.57
e1	U 570	E/S0	00 55 54.5	-00 55 15	0.0450	13.75	0.04	1.27		10.75	0.81	20.92	0.10	6.70	1.37	1	0.42	0.46	170.1	7.9	1.59	1.49	1.34	0.73

....Continue....

Table 7. b – Photometric and morphological parameters of galaxies in Abell 119(continue)

Galaxy	Name	Type	$\alpha(2000)$	$\delta(2000)$	z	m_T	Δm	$(B-r)$	$(V-r)$	R_{50}	ΔR_{50}	$\langle \mu_{50} \rangle$	$\Delta \mu_{50}$	n	Δn	Q	ε_e	ε_{max}	θ_e	$\Delta \theta$	$c_4(r_e)$	c_4^w	$\delta \mu_1$	$\delta \mu_2$
e2	D109	S0	00 55 53.6	-00 54 03	0.0365	16.13	0.04	1.22		1.42	0.10	18.91	0.19	2.40	9.41	0	0.06	0.57	75.8	15.3	0.16	2.94	1.76	0.76
f1		S0	00 55 40.8	-00 59 47		17.36	0.01		0.31	1.94	0.03	20.51	0.02	1.70	0.15	1	0.38	0.52	169.7	1.7		2.04	1.25	0.41
f2	D95	E	00 56 23.5	-00 59 12	0.0408	15.30	0.03		0.21	3.90	0.23	20.08	0.08	8.10	0.80	1	0.30	0.38	23.9	8.6	-0.30	-0.76	1.43	0.64
f3		S0	00 56 11.4	-00 58 13		17.52	0.03		0.20	1.87	0.08	20.72	0.08	0.70	0.26	0	0.15	0.27	11.0	4.7	0.25	-0.32	1.14	0.86
f4		E	00 56 08.7	-00 57 54	0.0478	16.89	0.09		0.33	3.52	0.61	21.43	0.25	10.00	5.81	0	0.15	0.22	58.5	7.5	-0.09	-0.96	0.65	1.10
f5		E	00 56 17.1	-00 57 11	0.0434	16.36	0.05		0.27	5.53	0.59	21.84	0.14	10.00	2.00	1	0.31	0.36	84.7	10.5	-0.19	0.99	1.29	0.71
f6	D116	E	00 55 51.2	-00 48 49		16.96	0.04		0.27	2.05	0.14	20.30	0.11	2.70	0.90	1	0.21	0.28	66.5	16.0	0.08	0.60	1.65	0.61
f7		E/S0	00 55 52.2	-00 48 18		16.84	0.01		0.40	4.32	0.09	21.76	0.05	10.00	2.70	0	0.14	0.24	142.7	27.6	1.81	1.26	1.36	0.82
g1	D106	E/S0	00 57 02.0	-00 52 47		15.84	0.03	1.24		2.21	0.13	19.59	0.08	4.50	0.85	1	0.32	0.39	155.1	5.0	0.55	0.32	1.31	0.74
g2	D107	S0	00 56 47.1	-00 52 41	0.0480	16.00	0.03	1.30		1.53	0.10	18.95	0.11	1.00	0.44	0	0.11	0.60	71.9	8.1	0.85	2.84	1.43	1.10
g3	U 588	E	00 57 02.0	-00 52 31	0.0443	13.19	0.03	1.49		13.26	0.70	20.82	0.07	6.10	0.86	1	0.23	0.28	142.7	9.5	1.23	0.91	1.24	0.73
g4	D104	E/S0	00 57 02.9	-00 52 23		16.73	0.04	1.17		1.32	0.07	19.35	0.08	1.60	0.40	1	0.11	0.26	139.8	13.3	0.36	-0.35	1.15	0.90
g5		Sa/0	00 57 05.1	-00 50 25		18.75	0.02	1.22		0.90	0.02	20.59	0.03	1.90	0.22	1	0.11	0.21	135.3	1.9	-2.93	-0.33	1.14	0.32
g6	D112	E	00 57 00.3	-00 49 31	0.0391	15.19	0.03	1.36		4.49	0.24	20.46	0.07	10.00	0.58	0	0.18	0.28	12.1	16.3	-0.16	0.58	1.21	0.73

Table 7. c – Photometric and morphological parameters of galaxies in Abell 1983

Galaxy	Name	Type	$\alpha(2000)$	$\delta(2000)$	z	m_T	Δm	$(B-r)$	$(V-r)$	R_{50}	ΔR_{50}	$\langle\mu_{50}\rangle$	$\Delta\mu_{50}$	n	Δn	Q	ε_e	ε_{max}	θ_e	$\Delta\theta$	$c_4(r_e)$	c_4^w	$\delta\mu_1$	$\delta\mu_2$
a1	D10	E	14 54 40.7	16 13 18	0.0434	14.65	0.04	1.60		3.79	0.30	19.58	0.125	4.60	1.58	1	0.02	0.12	150.0	103.1	0.21	0.40	1.29	0.71
b1		Sa/0	14 54 26.1	16 20 13		16.86	0.02	1.19		3.14	0.09	21.19	0.054	1.30	0.24	1	0.34	0.37	144.2	15.8	2.37	1.15	1.11	0.46
b2		E	14 54 22.6	16 20 48		16.56	0.02	1.35		1.05	0.05	18.55	0.183	2.10	4.45	0	0.14	0.14	136.8	74.0	0.33	0.33	1.86	1.13
b3		E	14 54 25.9	16 21 07		16.11	0.03	1.34		2.01	0.09	19.64	0.072	2.70	0.75	1	0.05	0.13	50.4	26.4	-0.35	-0.42	1.34	0.76
b4	I4516	E	14 54 23.4	16 21 19	0.0454	12.46	0.05	1.36		21.31	1.73	21.03	0.114	5.70	1.23	1	0.26	0.33	26.5	5.8	0.32	0.23	1.29	0.66
c1	D24	E	14 54 10.8	16 26 08	0.0449	15.11	0.02	1.36		2.55	0.08	19.17	0.054	2.40	0.33	1	0.18	0.19	47.7	27.4	0.03	0.13	1.20	0.54
d1		S0/a	14 51 21.5	16 25 44		17.72	0.02	1.21		1.52	0.03	20.68	0.041	1.00	0.16	1	0.30	0.31	19.3	21.5	0.25	-0.11	0.87	0.72
e1	D23	E/S0	14 55 29.7	16 27 46	0.0426	14.78	0.04	1.08		2.36	0.20	18.62	0.125	6.70	1.24	1	0.27	0.54	136.1	5.6	0.59	-0.01	1.36	0.66
f1	D35	S0/E	14 54 07.2	16 31 47	0.0458	14.56	0.04	1.33		3.18	0.21	19.03	0.114	2.80	1.17	1	0.41	0.55	117.6	3.0	3.51	1.69	1.49	0.66
g1		E	14 53 11.5	16 35 29		15.85	0.03	1.20		5.20	0.31	21.39	0.155	4.40	3.32	1	0.10	0.20	76.1	79.4	-0.02	-0.15	1.20	0.67
h1		E	14 52 59.7	16 40 44		17.64	0.00	1.17		0.85	0.01	19.32	0.030	2.30	0.41	0	0.06	0.20	128.9	131.1	-0.26	0.25	1.83	0.43
h2	D53	E	14 53 00.9	16 40 47	0.0468	15.28	0.04	1.32		2.76	0.17	19.53	0.096	3.30	0.69	1	0.01	0.13	137.3	146.2	-0.22	0.01	1.11	0.56
h3		E	14 52 59.1	16 40 59		16.73	0.06	1.20		2.25	0.25	20.52	0.209	2.40	1.91	1	0.02	0.06	124.3	115.6	-0.38	-0.05	1.18	0.80
h4	D55	S0/E	14 52 55.6	16 41 17	0.0424	15.87	0.03	1.01		2.92	0.12	20.10	0.083	1.40	0.47	0	0.21	0.33	1.0	23.7	-0.07	0.18	0.98	0.87
h5		E/S0	14 52 53.8	16 41 20		16.86	0.03	1.23		1.94	0.07	20.33	0.067	2.00	0.41	1	0.03	0.18	70.6	10.5	0.45	-0.11	1.11	0.72
h6	D57	E	14 52 55.0	16 41 24	0.0441	16.03	0.04	1.29		1.98	0.12	19.49	0.112	1.80	0.80	1	0.16	0.21	26.3	14.5	-0.05	0.11	1.09	0.86
h7	D54	E	14 52 57.7	16 41 49	0.0455	14.31	0.03	1.35		4.04	0.22	19.29	0.084	3.70	0.78	1	0.12	0.13	62.4	60.3	-1.34	-0.86	1.29	0.64
i1	D56	E	14 52 55.3	16 42 09	0.0440	13.72	0.03	1.34		21.20	1.08	22.04	0.070	9.90	0.50	1	0.10	0.10	60.6	86.6	0.67	-0.10	1.23	0.56
j1		S0	14 52 45.3	16 43 06		16.52	0.01	1.49		2.22	0.05	20.16	0.042	1.60	0.30	1	0.47	0.60	86.4	6.1	5.14	3.18	1.20	0.70
j2		S0/a	14 52 49.9	16 43 23		17.16	0.01	1.29		1.47	0.03	20.00	0.030	1.30	0.17	1	0.19	0.20	116.2	24.6	-0.30	0.04	1.05	0.65
j3		E/S0	14 52 43.4	16 43 28		15.82	0.02	1.23		2.78	0.09	20.06	0.055	2.20	0.36	1	0.28	0.29	126.2	9.5	-0.08	0.05	1.29	0.53
j4		SB0	14 52 42.7	16 43 45		16.90	0.02	1.21		2.41	0.06	20.79	0.043	1.20	0.21	0	0.26	0.28	102.3	33.0	0.48	0.33	0.85	0.56
k1	D78	E	14 49 57.0	16 48 30	0.0458	14.34	0.05	1.30		7.95	0.88	20.65	0.167	5.40	1.82	1	0.11	0.14	45.1	13.8	1.18	1.06	1.50	0.72
k2	D77	E	14 49 59.1	16 48 36	0.0461	14.59	0.02	1.30		6.80	0.28	20.76	0.067	4.20	0.41	1	0.37	0.43	157.0	6.7	-0.66	-0.92	1.33	0.60
l1	D80	E/S0	14 52 25.1	16 50 42	0.0474	14.66	0.04	1.16		2.52	0.21	18.55	0.113	8.60	1.09	1	0.21	0.38	117.8	6.8	-1.28	-0.22	1.23	0.70
m1	D84	E	14 52 43.2	16 54 13	0.0459	13.45	0.02	1.38		7.71	0.29	19.86	0.055	5.10	0.49	1	0.23	0.35	153.3	3.8	0.62	-0.96	1.27	0.63
n1	D81	S0	14 54 15.5	16 55 01	0.0462	14.83	0.02	1.35		3.26	0.11	19.33	0.067	1.70	0.38	1	0.43	0.53	105.0	19.4	3.14	2.88	1.08	0.59
o1	D94	S0	14 53 08.8	17 02 39	0.0444	14.05	0.01	1.45		5.28	0.09	19.59	0.027	2.50	0.16	1	0.44	0.58	169.3	7.2	0.74	1.03	1.11	0.49
p1	D105	E	14 52 22.8	17 07 18	0.0448	13.69	0.04	1.33		9.42	0.79	20.42	0.125	4.70	1.18	1	0.18	0.28	129.3	7.2	-0.13	0.15	1.46	0.62
q1		Sa/0	14 52 15.0	17 14 25		18.47	0.01	0.79		0.63	0.01	19.53	0.142	1.70	1.43	0	0.04	0.18	175.2	146.1		0.37	1.80	0.53
q2	D116	E	14 52 13.7	17 14 50	0.0454	14.13	0.02	1.31		6.95	0.29	20.30	0.068	3.50	0.49	1	0.27	0.30	96.3	11.5	3.81	0.80	1.35	0.65

Table 7. d – Photometric and morphological parameters of galaxies in DC 2103

Galaxy	Name	Type	$\alpha(2000)$	$\delta(2000)$	z	m_T	Δm	$(B-r)$	$(V-r)$	R_{50}	ΔR_{50}	$\langle \mu_{50} \rangle$	$\Delta \mu_{50}$	n	Δn	Q	ε_e	ε_{max}	θ_e	$\Delta \theta$	$c_4(r_e)$	c_4^w	$\delta \mu_1$	$\delta \mu_2$
a1		Sa/0	21 08 29.8	-39 55 47		18.51	0.06		-0.21	1.64	0.14	21.89	0.11	10.00	1.31	0	0.32	0.36	117.7	6.2		0.57	0.99	0.64
a2		E	21 09 27.9	-39 55 22		17.23	0.04		0.29	3.91	0.24	22.25	0.09	3.70	0.75	1	0.10	0.23	161.2	16.5	0.77	0.92	1.37	0.52
a3		E	21 08 28.7	-39 55 08		18.36	0.33		-0.36	4.42	0.67	23.39	0.26	9.80	20.00	0	0.23	0.28	106.8	38.3	0.41	0.57	1.30	1.09
a4		E	21 08 29.7	-39 54 59		16.02	0.02		-0.07	3.17	0.09	20.75	0.04	2.40	0.33	1	0.16	0.17	33.4	125.1	0.36	0.15	1.19	0.65
a5		E	21 08 41.2	-39 53 09		17.92	0.01		0.17	8.32	0.16	24.31	0.04	9.90	1.64	0	0.36	0.41	145.6	160.8	0.05	0.02	1.17	0.71
a6	D15	S0	21 08 39.1	-39 52 58	0.0499*	15.49	0.04		0.38	2.22	0.13	19.28	0.08	5.30	0.98	1	0.28	0.66	158.7	3.9	0.25	3.44	1.44	0.72
a7		E	21 08 33.4	-39 51 55		17.31	0.03		0.18	3.29	0.11	21.88	0.06	1.40	0.31	0	0.10	0.21	114.8	37.7	0.71	-0.12	0.83	0.84
a8		S0/a	21 09 20.8	-39 49 43		18.62	0.02		0.24	1.68	0.05	21.78	0.05	1.30	0.23	0	0.27	0.31	114.4	4.1	0.54	0.83	0.80	0.75
a9		S0/a	21 09 05.3	-39 48 00		17.28	0.06		-0.15	1.50	0.16	20.40	0.16	2.10	1.11	0	0.37	0.44	15.5	7.4	1.63	1.16	1.77	0.77
b1		SB0	21 06 00.0	-39 40 52		17.87	0.02		0.04	3.72	0.12	22.79	0.09	4.60	2.04	0	0.28	0.35	160.0	38.6	-0.20	-0.57	1.20	0.67
b2		E	21 06 08.4	-39 40 47		17.12	0.04		0.01	6.25	0.46	23.13	0.10	5.40	0.98	1	0.15	0.28	131.5	26.0	0.09	-0.07	1.29	0.74
b3	D40	E	21 06 01.0	-39 40 34	0.0497	14.48	0.03		0.27	7.92	0.39	20.96	0.07	9.40	0.80	1	0.17	0.21	70.5	32.5	0.39	-0.04	1.34	0.67
b4	D37	SB0/E	21 06 14.0	-39 40 15		16.23	0.08		0.12	3.07	0.46	20.75	0.20	6.70	2.40	0	0.24	0.29	80.6	48.6	1.16	-0.04	1.25	0.76
b5	D42	E/S0	21 05 40.8	-39 38 06	0.0488*	15.87	0.05		0.32	3.02	0.25	20.35	0.12	2.90	1.05	0	0.06	0.27	149.7	73.9	-0.58	0.08	1.23	0.88
b6	D39	E	21 06 02.4	-39 37 59	0.0526*	14.93	0.03		0.34	6.14	0.41	20.83	0.10	4.20	1.03	1	0.23	0.24	104.7	37.6	0.31	-0.74	1.36	0.65
b7	D38	E	21 06 05.3	-39 37 52	0.0523*	14.53	0.02		0.18	7.20	0.21	20.88	0.04	10.00	0.30	1	0.17	0.35	10.0	121.3	1.14	1.08	1.28	0.76
b8	D54	S0/E	21 06 01.6	-39 37 20		16.45	0.04		0.11	1.78	0.15	19.77	0.11	6.90	1.06	1	0.24	0.48	87.6	5.7		1.42	1.38	0.54
b9		Sa/0	21 06 00.0	-39 37 14		17.79	0.03		0.01	3.20	0.13	22.46	0.06	2.50	0.39	1	0.12	0.19	11.7	20.2	0.24	0.10	1.36	0.60
b10	D55	E	21 05 57.5	-39 36 55		15.12	0.03		0.30	10.26	0.61	22.13	0.09	3.80	0.83	1	0.30	0.45	129.1	8.2	-0.48	-0.90	1.40	0.71
b11		S0/E	21 06 27.6	-39 36 38		18.26	0.03		-0.14	2.25	0.08	21.94	0.06	1.80	0.41	1	0.26	0.30	126.5	3.5	0.50	0.26	1.09	0.57
b12		E	21 05 47.6	-39 36 02		18.25	0.03		-0.02	1.08	0.04	20.46	0.05	4.90	0.27	0	0.16	0.18	105.4	7.9		0.85	0.67	0.90
b13		S0/a	21 06 13.8	-39 35 23		17.98	0.03		-0.31	1.63	0.06	21.10	0.05	3.40	0.48	1	0.43	0.44	109.8	3.1	0.50	0.98	1.38	0.49
b14		Sa/0	21 05 53.7	-39 35 04		18.27	0.02		0.04	1.76	0.04	21.52	0.03	1.30	0.15	0	0.20	0.23	0.2	33.2	1.38	0.06	0.85	0.25
b15	D52	E	21 06 32.6	-39 34 26		16.47	0.01		0.09	3.71	0.10	21.33	0.03	6.80	0.34	1	0.07	0.18	147.5	81.6	-0.30	-0.41	1.37	0.48
b16		SB0	21 06 25.1	-39 33 01		16.78	0.03		0.09	2.38	0.10	20.77	0.06	1.90	0.42	1	0.24	0.27	61.6	70.1	2.60	1.14	1.08	0.85
b17		S0	21 06 32.2	-39 30 54		17.54	0.04		-0.03	2.09	0.13	21.18	0.08	9.90	0.94	1	0.31	0.31	16.6	62.5	1.71	0.49	1.13	0.68
c1	D47	S0/a	21 07 49.7	-39 34 48		16.72	0.02		0.22	2.55	0.05	20.76	0.04	1.00	0.15	0	0.25	0.41	28.6	8.9	0.71	0.35	0.84	0.63
c2		E	21 07 55.9	-39 34 33		18.19	0.03		0.09	0.96	0.05	20.15	0.08	9.80	2.54	0	0.27	0.28	4.9	9.5		-0.01	1.66	0.44
c3		E	21 07 23.8	-39 32 56		17.75	0.05		0.11	1.99	0.18	21.28	0.14	3.70	1.56	1	0.03	0.15	120.4	95.9	0.16	-0.12	1.55	0.86
c4	D61	S0/E	21 07 41.2	-39 31 39	0.0508	14.43	0.03		0.40	6.61	0.30	20.41	0.07	2.40	0.55	1	0.51	0.52	111.0	9.0	0.78	-0.21	1.41	0.56
c5	D62	S0	21 07 27.4	-39 31 18	0.0505*	16.41	0.01		0.32	2.15	0.06	20.06	0.05	1.90	0.38	0	0.04	0.29	19.9	50.9	0.08	-0.17	1.72	0.56
c6	D60	S0	21 08 08.9	-39 31 13	0.0515*	16.04	0.11		0.30	2.51	0.58	20.01	0.33	10.00	6.80	0	0.11	0.43	88.2	35.2	0.08	-0.02	1.08	0.74
c7	D63	E	21 07 26.5	-39 31 02	0.0495*	16.52	0.02		0.30	1.60	0.05	19.57	0.05	2.30	0.38	1	0.15	0.27	126.1	13.8	0.08	0.46	1.31	0.62
c8	D76	E/S0	21 07 30.7	-39 29 52	0.0504*	14.68	0.03		0.33	5.73	0.26	20.40	0.07	3.30	0.65	1	0.26	0.27	23.4	30.6	-0.28	-0.28	1.26	0.62
c9	D77	SB0	21 07 29.6	-39 28 59		15.92	0.19		0.36	2.22	0.47	19.62	0.69	10.00	38.15	0	0.12	0.26	179.7	44.0	1.50	-0.12	1.78	0.99
c10		Sa/0	21 07 31.5	-39 28 19		18.27	0.02		0.10	1.72	0.05	21.44	0.05	1.80	0.32	1	0.31	0.33	9.9	14.0	1.20	-0.13	1.28	0.64
c11		E/S0	21 07 40.8	-39 28 11		18.47	0.03		0.05	1.85	0.10	21.77	0.08	2.80	0.70	1	0.14	0.18	72.9	11.3	-0.41	-1.45	1.33	0.83
c12	D74	S0	21 07 41.7	-39 28 00	0.0483	16.81	0.02		0.12	2.10	0.07	20.45	0.05	1.10	0.15	0	0.06	0.25	72.6	17.9	-0.77	0.38	0.58	0.54
c13	D73	E	21 07 45.5	-39 27 37	0.0493*	14.44	0.04		0.36	10.79	0.81	21.56	0.10	5.40	1.00	1	0.20	0.28	34.5	19.6	-0.84	-0.53	1.46	0.67
c14	D71	E	21 07 59.5	-39 26 42	0.0491*	15.85	0.03		0.34	3.24	0.23	20.36	0.09	9.20	0.75	1	0.17	0.20	163.0	63.7	0.03	1.35	1.34	0.51
c15		S0	21 07 54.7	-39 25 29		17.10	0.03		0.11	1.98	0.09	20.62	0.08	1.90	0.57	0	0.37	0.64	81.0	5.3	5.54	4.73	1.34	0.80

Table 7. e – Photometric and morphological parameters of galaxies in Abell 3125

Galaxy	Name	Type	$\alpha(2000)$	$\delta(2000)$	z	m_T	Δm	$(B-r)$	$(V-r)$	R_{50}	ΔR_{50}	$\langle \mu_{50} \rangle$	$\Delta \mu_{50}$	n	Δn	Q	ε_e	ε_{max}	θ_e	$\Delta \theta$	$c_4(r_e)$	c_4^w	$\delta \mu_1$	$\delta \mu_2$
a1	D9	E	03 26 53.8	-53 54 08	0.0615*	15.58	0.02		0.24	4.43	0.19	20.85	0.068	4.60	0.56	1	0.03	0.21	133.5	53.5	-0.28	-0.33	1.30	0.63
a2		E	03 26 19.8	-53 47 47		16.21	0.03		0.32	8.29	0.46	22.79	0.072	6.60	0.71	1	0.27	0.34	28.8	16.5	0.62	1.15	1.22	0.73
b1		E	03 29 51.8	-53 34 17		17.17	0.03		0.20	2.95	0.14	21.77	0.070	2.70	0.47	1	0.08	0.19	0.4	41.8	0.58	-0.01	1.07	0.54
b2		E	03 29 51.8	-53 34 07		17.63	0.01		0.22	1.31	0.03	20.21	0.030	7.30	0.77	0	0.19	0.27	142.6	11.7		0.55	1.51	0.84
b3		S0	03 28 54.7	-53 29 15		18.06	0.03		0.15	1.49	0.08	20.99	0.097	1.10	0.42	0	0.15	0.25	51.3	9.0		-0.30	1.63	0.57
b4		S0	03 28 42.3	-53 29 14		16.57	0.02		0.33	2.22	0.04	20.35	0.030	1.00	0.16	0	0.50	0.72	78.7	1.4		6.20	0.76	0.63
b5	D46	E	03 29 03.7	-53 28 26	0.0594	14.65	0.04		0.23	7.02	0.49	20.90	0.098	8.40	1.01	1	0.12	0.14	69.7	5.9	0.46	0.08	1.39	0.70
c1		E/S0	03 28 22.2	-53 27 29		17.13	0.05	1.20		2.34	0.20	21.06	0.138	3.50	1.26	1	0.18	0.30	19.5	6.9	0.53	-0.26	1.31	0.96
c2	D50	SB0/a	03 27 37.0	-53 27 24		16.27	0.04	1.37		2.69	0.15	20.44	0.098	2.60	0.84	1	0.25	0.33	123.1	11.6	3.74	0.48	1.05	0.89
c3		E	03 27 06.6	-53 27 21		17.34	0.03	1.31		2.25	0.12	21.15	0.085	2.50	0.67	1	0.13	0.14	44.4	57.2	-0.71	0.091	1.30	0.84
c4	D49	S0	03 27 47.1	-53 26 58		16.49	0.01	1.34		1.84	0.03	19.84	0.027	4.00	0.23	1	0.14	0.46	33.7	2.9	-0.14	0.71	1.28	0.83
c5	D48	E/S0	03 27 45.9	-53 26 30	0.0579	15.63	0.03	1.36		2.74	0.14	19.89	0.083	2.90	0.71	1	0.23	0.33	86.4	20.2	1.01	0.89	1.25	0.82
c6	D47	E	03 27 52.2	-53 26 11	0.0590	14.40	0.06	1.34		13.10	1.79	21.99	0.209	10.00	4.64	1	0.24	0.30	96.0	9.8	1.84	1.09	1.30	0.79
c7	D52	E	03 27 23.7	-53 25 34	0.0642	15.08	0.05	1.37		10.79	1.55	22.28	0.267	10.00	14.74	0	0.13	0.20	21.8	118.9	-1.64	-0.93	1.23	0.84
c8		E	03 27 24.4	-53 25 23		14.58	0.09	1.40		7.34	1.53	21.00	0.296	10.00	4.95	1	0.10	0.22	164.3	25.4	1.49	0.91	1.33	0.88
c9		E	03 27 48.3	-53 25 23		17.57	0.04	1.30		2.34	0.17	21.51	0.109	9.30	1.20	1	0.14	0.16	18.5	26.0	-0.48	-0.28	1.42	0.84
c10	D51	E	03 27 24.9	-53 25 14	0.0623*	16.73	0.07	1.43		2.28	0.32	20.59	0.314	2.40	3.65	1	0.13	0.20	128.2	22.2	-0.07	-0.95	1.41	0.71
c11		E/S0	03 28 18.5	-53 25 14		17.86	0.03	1.26		1.97	0.08	21.41	0.069	1.60	0.37	0	0.14	0.21	42.7	2.6	-0.01	-0.44	1.34	0.66
c12	D62	S0	03 27 42.5	-53 24 47		16.60	0.01	1.34		1.64	0.02	19.74	0.025	1.30	0.08	0	0.44	0.65	131.7	2.3		3.99	0.89	0.32
c13		S0	03 27 45.4	-53 24 03		17.08	0.04	1.28		0.95	0.05	19.09	0.098	1.90	0.64	0	0.23	0.56	98.9	4.6		5.36	1.48	0.47
c14	D60	E	03 27 54.7	-53 22 19	0.0585	14.52	0.01	1.34		7.26	0.18	20.84	0.030	7.70	0.32	1	0.06	0.06	5.5	15.8	-0.21	-0.15	1.37	0.72
c15	D67	E/S0	03 27 51.0	-53 21 43		16.95	0.02	1.23		2.11	0.05	20.64	0.043	1.20	0.22	0	0.14	0.19	169.9	19.9	-0.45	-0.30	1.01	0.70
c16		S0	03 28 00.4	-53 20 10		17.23	0.07	1.33		1.71	0.19	20.46	0.197	1.20	0.93	0	0.21	0.59	99.0	1.4		2.29	1.50	0.78
d1		E	03 23 38.4	-53 23 28		18.27	0.00		0.28	0.78	0.01	19.71	0.026	9.80	0.72	0	0.05	0.29	24.9	4.6		1.16	1.78	0.36
d2		E	03 23 40.9	-53 22 12		18.03	0.03		0.28	1.05	0.04	20.23	0.169	5.40	6.81	0	0.31	0.32	138.0	20.0		0.40	1.37	0.29
d3		E	03 23 55.3	-53 22 00		18.01	0.01		0.26	0.87	0.01	19.80	0.169	1.20	2.31	0	0.15	0.15	74.9	105.3		-0.41	1.72	0.38
d4		E	03 23 42.6	-53 21 57		18.38	0.03		0.34	1.15	0.07	20.75	0.084	1.10	0.20	0	0.05	0.19	6.0	10.4		0.62	0.37	0.75
d5	D76	S0	03 23 51.3	-53 19 05		16.04	0.04		0.23	2.26	0.13	19.87	0.100	1.50	0.64	0	0.20	0.48	84.4	12.4	1.12	2.22	0.96	1.10
d6	D75	Sa/0	03 24 04.6	-53 18 54		16.79	0.02		0.23	2.05	0.06	20.40	0.055	0.90	0.19	0	0.24	0.54	38.6	7.9	0.01	0.50	1.27	0.58
d7		S0/E	03 23 38.7	-53 18 33		17.43	0.05		0.23	1.69	0.08	20.55	0.085	1.80	0.65	0	0.22	0.23	5.1	31.6	1.07	0.24	1.09	0.22
d8	D77	S0/a	03 23 44.6	-53 17 33	0.0588*	16.03	0.01		0.17	2.82	0.05	20.29	0.038	1.40	0.12	1	0.17	0.19	143.5	29.5	-0.16	-0.55	0.93	0.31
d9	D83	S0/a	03 23 44.2	-53 17 06		16.66	0.03		0.29	2.02	0.11	20.20	0.098	1.40	0.51	0	0.34	0.60	64.8	1.8	3.69	3.73	1.16	1.09
d10		E/S0	03 24 21.1	-53 15 59		18.13	0.08		0.28	1.78	0.28	21.47	0.071	1.60	1.91	0	0.04	0.21	163.3	43.4	-0.65	-0.22	1.71	1.03
d11	D84	Sa/0	03 23 44.2	-53 15 25		16.85	0.03		0.23	2.11	0.09	20.52	0.071	0.90	0.25	0	0.28	0.57	33.0	3.8		1.23	1.45	0.60
e1		S0/a	03 27 13.8	-53 13 00		17.83	0.03		0.18	1.21	0.05	20.32	0.070	3.50	0.73	1	0.30	0.44	119.5	3.1		0.60	1.40	0.52
e2	D88	E	03 27 38.4	-53 11 15	0.0599	14.74	0.05		0.20	6.28	0.58	20.65	0.155	3.20	1.64	1	0.09	0.21	116.0	47.7	-0.52	-0.98	1.43	0.57
e3	D95	E	03 27 22.0	-53 10 04	0.0601	15.63	0.03		0.22	4.57	0.24	20.97	0.071	4.60	0.62	1	0.19	0.24	104.2	7.8	0.83	0.51	1.34	0.52
e4	D94	S0	03 27 21.4	-53 09 05	0.0662	15.85	0.04		0.20	3.99	0.30	20.86	0.100	10.00	0.86	0	0.17	0.39	30.8	39.5	0.11	0.65	1.44	0.53
e5	D93	S0	03 27 24.2	-53 08 27	0.0582	15.50	0.03		0.26	3.79	0.14	20.43	0.068	1.40	0.33	0	0.32	0.69	38.0	5.0	2.32	3.21	1.11	0.82
e6	D96	S0	03 26 38.9	-53 08 17	0.0598	15.52	0.02		0.25	2.46	0.07	19.51	0.043	1.50	0.23	1	0.44	0.74	66.5	1.0		2.09	1.33	0.63

....Continue....

Table 7. e – Photometric and morphological parameters of galaxies in Abell 3125(continue)

Galaxy	Name	Type	$\alpha(2000)$	$\delta(2000)$	z	m_T	Δm	$(B-r)$	$(V-r)$	R_{50}	ΔR_{50}	$\langle\mu_{50}\rangle$	$\Delta\mu_{50}$	n	Δn	Q	ε_e	ε_{max}	θ_e	$\Delta\theta$	$c_4(r_e)$	c_4^w	$\delta\mu_1$	$\delta\mu_2$
f1		Sa/0	03 24 10.0	-53 11 28		18.09	0.02		0.16	1.87	0.05	21.48	0.043	1.00	0.18	0	0.17	0.33	133.4	4.3		2.50	0.77	0.72
f2		S0/a	03 24 01.7	-53 08 18		17.92	0.02		0.24	1.57	0.03	20.98	0.030	1.10	0.15	1	0.33	0.50	99.3	3.2		1.78	0.97	0.68
f3	D97	E/S0	03 24 01.7	-53 08 18		16.33	0.02		0.13	2.48	0.06	20.35	0.042	1.20	0.20	1	0.23	0.32	116.7	3.8	0.54	-0.32	1.08	0.73
f4		S0	03 24 33.7	-53 07 42		17.16	0.04		0.24	2.29	0.16	21.00	0.113	1.00	0.41	0	0.06	0.11	137.5	44.4	-1.47	0.44	1.29	0.90
f5		E	03 24 11.6	-53 06 56		16.91	0.04		0.18	1.71	0.10	20.13	0.100	2.00	0.76	1	0.22	0.27	146.0	33.3		-0.04	1.63	0.49
f6		E/S0	03 24 51.9	-53 06 23		18.26	0.04		0.17	1.10	0.08	20.57	0.100	1.90	0.43	0	0.26	0.33	26.1	6.1	1.63	0.43	1.73	0.71
f7		S0/a	03 24 20.3	-53 06 08		17.86	0.05		0.33	1.22	0.10	20.40	0.141	1.20	0.68	0	0.16	0.35	71.2	7.3	0.99	1.37	1.72	0.48
f8		E	03 23 50.1	-53 05 54		16.84	0.07		0.22	3.78	0.42	21.78	0.197	3.70	2.64	1	0.15	0.17	169.7	20.2	0.66	0.15	1.22	0.82
f9	D102	S0	03 23 39.8	-53 05 05		17.02	0.03		0.23	1.51	0.07	20.00	0.072	1.30	0.36	0	0.30	0.45	48.1	8.2	1.31	1.24	1.53	0.62
f10		E/S0	03 24 25.5	-53 05 04		17.84	0.04		0.29	1.65	0.08	20.99	0.083	1.50	0.34	0	0.16	0.17	118.4	5.0		0.98	0.75	1.21
f11		E	03 24 47.4	-53 02 23		15.02	0.07		0.28	13.16	1.51	22.61	0.167	10.00	2.38	1	0.36	0.36	120.5	5.2	0.06	0.04	1.31	0.65
g1		SB0	03 22 59.9	-53 06 59		16.20	0.00		0.24	1.92	0.01	19.67	0.054	0.90	0.26	0	0.12	0.22	11.4	69.0	0.93	0.85	1.76	1.12
g2		E	03 23 50.1	-53 05 54		16.81	0.03		0.42	4.33	0.22	22.00	0.071	4.40	0.56	1	0.18	0.24	169.9	13.4	-1.46	0.21	1.34	0.60
g3	D103	S0	03 23 10.6	-53 05 08	0.0594*	16.55	0.03		0.21	1.32	0.07	19.14	0.072	3.40	0.58	1	0.18	0.71	101.6	4.5		5.35	1.19	0.65
g4	D102	S0/a	03 23 39.8	-53 05 05		17.10	0.03		0.42	1.41	0.05	19.86	0.055	4.40	0.25	0	0.26	0.47	41.1	21.5		1.63	1.38	0.75
g5	D104	E	03 22 58.0	-53 04 39	0.0600*	14.58	0.03		0.24	11.11	0.78	21.68	0.109	5.80	1.10	1	0.45	0.48	60.1	8.4	-1.49	-0.43	1.42	0.70
h1		E/S0	03 30 11.9	-52 56 19		17.06	0.02	1.17		2.49	0.07	21.09	0.043	2.10	0.31	1	0.29	0.34	144.0	9.9	0.88	0.76	1.21	0.60
h2		Sa/0	03 31 01.7	-52 54 36		17.42	0.01	1.21		2.23	0.02	21.19	0.026	1.00	0.09	1	0.06	0.09	147.0	37.1	0.06	-0.16	0.86	0.45
h3	D129	S0	03 30 56.3	-52 51 20	0.0624	15.70	0.06	1.34		4.36	0.56	20.94	0.171	10.00	1.93	0	0.02	0.11	76.3	126.2	0.25	-0.01	1.37	0.60
h4	D130	E	03 30 45.8	-52 51 03	0.0627	14.61	0.04	1.45		5.79	0.45	20.42	0.101	7.40	1.21	1	0.21	0.22	165.4	17.4	1.11	-0.27	1.35	0.71
h5		E	03 30 47.1	-52 50 41		17.62	0.04	1.24		2.59	0.12	21.67	0.096	0.90	0.34	0	0.19	0.22	69.0	5.4	0.12	-0.28	1.00	0.44
h6	D128	E	03 31 00.9	-52 49 21	0.0635	15.70	0.06	1.43		4.39	0.49	20.94	0.155	10.00	2.26	1	0.15	0.24	106.8	15.1	0.72	0.10	1.34	0.59
h7	D140	E	03 31 05.0	-52 48 47	0.0631	15.08	0.04	1.46		4.76	0.34	20.45	0.113	3.80	1.25	1	0.34	0.38	116.7	7.1	-1.23	-1.65	1.33	0.55
h8	D142	S0/E	03 30 27.5	-52 46 51	0.0593	16.10	0.04	1.50		1.83	0.10	19.48	0.098	1.30	0.50	1	0.23	0.44	47.1	4.3		0.52	1.58	0.64
h9	D138	SB0	03 31 35.2	-52 46 51	0.0610	15.77	0.02	1.48		2.40	0.04	19.73	0.038	1.80	0.16	1	0.39	0.62	93.5	5.7	4.99	3.03	0.92	0.46
h10		Sa/0	03 30 42.5	-52 46 48	0.0599	17.07	0.05	1.30		1.83	0.16	20.43	0.155	1.40	0.82	0	0.19	0.23	97.9	51.7		-0.14	1.36	1.09
h11		S0	03 31 28.3	-52 46 30		17.79	0.02	1.52		1.21	0.03	20.33	0.042	1.80	0.20	0	0.30	0.45	6.6	7.4		2.17	0.94	0.83
i1	D162	S0	03 27 30.3	-52 41 29	0.0594	16.60	0.02		0.24	2.96	0.07	21.04	0.042	1.90	0.26	1	0.12	0.26	103.8	24.7	0.27	0.62	0.99	0.56
i2		E	03 27 41.7	-52 41 20	0.0622	16.75	0.03		0.30	2.85	0.12	21.10	0.072	1.50	0.45	0	0.17	0.31	133.6	16.9	-0.41	0.03	1.01	0.69
i3	D163	SB0	03 27 31.3	-52 40 44		16.48	0.03		0.25	2.29	0.12	20.38	0.097	1.20	0.43	1	0.32	0.44	138.5	15.0	4.60	-0.63	0.95	0.89
i4	I1942	E	03 27 53.7	-52 40 34	0.0614	13.66	0.03		0.25	18.41	1.15	21.93	0.109	3.00	0.87	1	0.29	0.35	169.1	15.7	2.49	0.83	1.44	0.65

Table 7. f – Photometric and morphological parameters of galaxies in Abell 1069

Galaxy	Name	Type	$\alpha(2000)$	$\delta(2000)$	z	m_T	Δm	$(B-r)$	$(V-r)$	R_{50}	ΔR_{50}	$\langle \mu_{50} \rangle$	$\Delta \mu_{50}$	n	Δn	Q	ε_e	ε_{max}	θ_e	$\Delta \theta$	$c_4(r_e)$	c_4^w	$\delta \mu_1$	$\delta \mu_2$
a1		Sa/0	10 37 23.1	-09 16 10		19.43	0.05	1.38		2.13	0.15	23.04	0.18	1.00	0.94	0	0.44	0.47	53.3	6.4	2.47	1.37	1.39	0.28
a2		E	10 37 53.7	-09 09 05		17.29	0.04	1.31		1.59	0.09	20.31	0.11	1.50	0.74	1	0.17	0.25	20.0	14.8	0.87	-0.02	1.53	0.70
a3	D3	S0	10 37 31.7	-09 08 56	0.0636*	16.38	0.12	1.42		1.84	0.42	19.75	0.33	2.00	8.87	0	0.26	0.59	39.8	1.6	1.83	4.26	1.64	0.63
a4		Sa/0	10 37 48.7	-09 07 53		19.49	0.04	1.29		1.83	0.11	22.81	0.12	1.50	0.82	1	0.29	0.35	93.5	10.6	2.32	1.81	1.48	0.39
a5		S0/a	10 37 22.7	-09 03 23		18.70	0.03	1.36		1.28	0.03	21.32	0.05	0.90	0.23	1	0.39	0.43	71.7	3.1		0.97	0.92	0.20
b1	D14	E	10 40 53.1	-08 51 01	0.0549*	15.67	0.04		0.25	3.88	0.29	20.66	0.13	3.00	1.39	1	0.42	0.47	162.2	5.1	0.53	0.23	1.35	0.71
b2	D15	E	10 40 25.1	-08 50 14	0.0662	14.61	0.06		0.31	8.43	1.11	21.26	0.18	7.90	2.33	1	0.11	0.17	67.9	8.1	-0.56	0.15	1.53	0.71
c1	D21	E	10 39 43.4	-08 41 13	0.0649	13.62	0.04	1.55		19.62	1.05	22.08	0.07	4.20	0.46	1	0.14	0.27	75.5	22.4	1.05	-1.12	1.11	0.48
c2	D20	E/S0	10 39 50.2	-08 41 03	0.0660	16.15	0.09	1.46		1.99	0.36	19.69	0.29	1.60	3.67	0	0.13	0.26	171.9	41.9	0.03	-0.23	1.93	0.72
c3	D19	E	10 39 53.1	-08 40 37	0.0602	15.47	0.03	1.42		3.32	0.16	20.11	0.08	2.40	0.60	1	0.03	0.06	26.3	77.4	-0.46	0.14	1.20	0.71
c4		SB0/E	10 39 49.9	-08 37 48	0.0607	16.20	0.04	1.45		2.84	0.14	20.50	0.07	2.20	0.51	1	0.15	0.18	109.7	65.8	2.72	-0.50	1.07	0.66
c5	D25	E	10 39 44.1	-08 34 56	0.0678	15.54	0.03	1.44		3.75	0.18	20.45	0.07	3.30	0.68	1	0.17	0.24	127.1	3.2	0.44	-0.15	1.22	0.58
c6		Sa/0	10 40 02.7	-08 32 40	0.0671	16.50	0.02	1.38		3.07	0.05	20.95	0.04	0.70	0.14	0	0.43	0.61	67.1	2.2	3.65	1.57	0.92	0.66
c7	D29	E	10 39 37.7	-08 32 32	0.0669	14.72	0.05	1.55		9.45	0.89	21.62	0.13	5.20	1.57	1	0.16	0.21	60.8	28.1	-0.75	-0.52	1.48	0.70
c8		S0	10 39 41.0	-08 31 53	0.0683	16.37	0.02	1.39		3.60	0.11	21.16	0.05	1.80	0.37	1	0.37	0.44	171.9	2.6	2.49	0.57	1.31	0.65
d1		S0/a	10 39 53.2	-08 20 23		18.62	0.07		0.20	1.08	0.09	20.88	0.19	2.20	2.39	1	0.29	0.36	94.4	9.4		1.22	1.14	0.23
d2		E	10 39 49.8	-08 19 55		18.60	0.08		0.37	0.99	0.13	20.65	0.20	2.50	4.72	1	0.09	0.10	128.6	10.1		0.35	1.61	0.47
d3	D34	E	10 39 55.7	-08 18 49		15.31	0.06		0.26	4.06	0.62	20.37	0.25	5.00	4.30	1	0.26	0.30	149.0	36.8	1.06	0.74	1.38	0.78
d4		E/S0	10 40 20.1	-08 17 03		18.16	0.04		0.24	1.32	0.06	20.82	0.07	2.00	0.49	1	0.07	0.22	69.4	17.4	0.97	0.14	1.15	0.46
e1		E?	10 41 51.8	-08 16 47		19.29	0.04	1.16		1.30	0.08	21.88	0.11	1.30	0.58	1	0.06	0.13	23.0	16.8		-0.53	1.42	0.72
e2	D39	E/S0	10 41 45.8	-08 14 54	0.0649*	16.03	0.04	1.47		2.31	0.13	19.89	0.09	1.40	0.52	1	0.28	0.50	124.3	9.5	-0.14	0.25	1.40	0.72
e3		Sa/0	10 42 01.4	-08 14 35		17.54	0.05	1.40		1.96	0.13	21.01	0.13	1.10	0.65	1	0.29	0.43	174.6	3.7	0.81	0.53	1.51	0.62
e4		E/S0	10 42 05.2	-08 14 23		18.03	0.05	1.39		1.56	0.11	21.03	0.15	1.70	1.22	1	0.09	0.17	139.4	17.2	0.30	1.03	1.63	0.45
e5		SB0	10 41 51.3	-08 13 34		16.39	0.02	1.41		3.93	0.08	21.37	0.03	1.30	0.17	1	0.18	0.37	26.2	70.1	0.19	0.80	0.95	0.50
e6		E	10 41 56.6	-08 13 18		18.14	0.04	1.23		0.80	0.03	19.74	0.17	2.60	8.56	0	0.19	0.22	122.7	142.2		-0.10	1.04	0.20
e7		Sa/0	10 41 44.5	-08 13 10		16.89	0.04	1.40		3.24	0.15	21.47	0.08	1.10	0.39	0	0.31	0.47	53.4	8.5	1.03	0.25	0.89	0.75
e8	D38	E	10 41 52.7	-08 12 30	0.0638*	13.72	0.03	1.45		18.42	1.00	22.03	0.07	5.90	0.74	1	0.36	0.46	128.6	2.9	-0.81	-1.44	1.32	0.69
e9		E	10 41 58.5	-08 09 36		17.91	0.03	1.40		1.60	0.06	20.99	0.07	1.30	0.42	1	0.10	0.17	147.5	26.0		0.33	1.40	0.42
e10		S0	10 41 37.1	-08 07 31		16.85	0.11	1.41		1.63	0.36	19.97	0.33	1.50	7.82	0	0.21	0.54	40.1	5.0		3.51	2.00	0.54
f1		S0?	10 38 03.0	-08 14 42		18.89	0.10		0.30	1.23	0.26	21.36	0.33	1.20	9.37	1	0.23	0.40	94.1	4.8		2.85	1.75	0.59
f2		E	10 38 35.0	-08 13 43		17.20	0.02		0.14	1.33	0.06	19.88	0.15	4.00	5.29	0	0.04	0.07	114.6	127.6		0.01	1.92	0.55
f3		S0/E	10 38 05.1	-08 12 02		18.70	0.05		0.31	1.29	0.14	21.24	0.20	2.00	5.70	1	0.23	0.34	27.3	5.1		-0.06	1.57	0.89
f4		E	10 38 06.7	-08 11 59		18.28	0.08		0.29	1.11	0.17	20.57	0.26	2.40	3.42	1	0.10	0.18	73.4	22.0		-0.22	1.62	0.79
f5		E	10 38 19.0	-08 11 39		17.11	0.04		0.27	2.65	0.19	21.26	0.11	3.20	1.22	1	0.19	0.32	96.7	3.2	0.86	0.43	1.25	0.93
f6		E	10 30 10.0	-08 11 26		16.35	0.09		0.26	8.10	1.78	22.60	0.30	10.80	5.02	1	0.10	0.18	85.5	62.0	0.07	-0.27	1.27	0.66
f7	D40	S0	10 38 33.7	-08 11 23	0.0641*	15.76	0.03		0.22	3.33	0.14	20.39	0.08	1.50	0.55	1	0.31	0.41	51.9	10.9	1.25	1.48	1.10	0.78
f8		E/S0	10 38 00.4	-08 11 10		18.27	0.04		0.23	1.32	0.08	20.93	0.12	1.20	0.67	1	0.12	0.24	34.7	15.8		0.14	1.41	0.48
f9	D43	S0	10 38 12.4	-08 10 17		16.12	0.02		0.25	3.25	0.07	20.68	0.05	0.80	0.19	1	0.53	0.69	1.4	0.9	7.27	3.90	0.93	0.65
f10		E	10 38 05.3	-08 07 46		18.43	0.03		0.19	1.61	0.06	21.51	0.06	2.20	0.51	1	0.09	0.12	90.7	50.9		-0.39	1.30	0.62
f11		S0	10 38 36.9	-08 07 04		18.02	0.03		0.32	1.42	0.06	20.80	0.08	0.90	0.34	1	0.32	0.47	6.6	4.6	4.47	4.33	1.16	0.73

....Continue....

Table 7. f – Photometric and morphological parameters of galaxies in Abell 1069(continue)

Galaxy	Name	Type	$\alpha(2000)$	$\delta(2000)$	z	m_T	Δm	$(B-r)$	$(V-r)$	R_{50}	ΔR_{50}	$\langle\mu_{50}\rangle$	$\Delta\mu_{50}$	n	Δn	Q	ε_e	ε_{max}	θ_e	$\Delta\theta$	$c_4(r_e)$	c_4^w	$\delta\mu_1$	$\delta\mu_2$
f12		S0	10 38 12.7	−08 06 00		18.97	0.05	0.26	1.08	0.09	21.17	0.16	1.40	1.03	1	0.28	0.36	172.3	2.6		1.31	1.60	0.63	
g1		E	10 40 59.6	−08 03 15		17.53	0.08	0.26	1.02	0.14	19.65	0.25	2.40	2.90	0	0.16	0.23	105.7	35.8		0.67	1.71	0.60	
g2		E/S0	10 40 29.2	−08 02 11		18.54	0.05	0.35	1.49	0.10	21.46	0.11	1.90	0.73	1	0.24	0.31	149.8	7.4	0.54	−0.12	1.41	0.69	
g3		E/S0	10 40 23.5	−08 01 50		18.15	0.06	0.32	1.30	0.15	20.81	0.21	1.50	1.35	0	0.12	0.19	52.4	9.7		−0.46	1.75	0.71	
g4		E/S0	10 40 34.5	−08 00 52		16.19	0.06	0.30	2.28	0.27	19.97	0.19	3.10	1.89	1	0.26	0.39	60.1	8.5	1.43	0.27	1.32	1.14	
g5	D46	E	10 40 35.7	−08 00 00	0.0648*	14.54	0.02	0.32	9.18	0.36	21.38	0.06	3.80	0.54	1	0.08	0.09	46.9	20.2	−1.02	−0.53	1.28	0.64	
g6		E	10 40 18.6	−07 56 18		17.69	0.04	0.47	1.82	0.10	21.03	0.09	1.90	0.52	1	0.01	0.06	127.3	196.9	−0.98	−0.17	1.15	0.87	
g7		E	10 40 34.6	−07 56 00		17.01	0.07	0.32	2.05	0.30	20.60	0.22	5.20	3.13	1	0.05	0.14	26.0	5.9	0.09	−0.07	1.39	1.05	
g8		E	10 41 03.9	−07 55 31		16.34	0.03	0.34	3.02	0.16	20.79	0.08	3.60	0.85	1	0.06	0.09	129.2	53.2	−0.68	0.27	1.25	0.71	
g9		Ep	10 40 40.1	−07 54 30		16.46	0.03	0.21	2.63	0.17	20.54	0.13	7.40	4.23	1	0.16	0.38	129.2	17.8	1.41	1.32	1.47	0.83	

Table 7. g – Photometric and morphological parameters of galaxies in Abell 2670

Galaxy	Name	Type	$\alpha(2000)$	$\delta(2000)$	z	m_T	Δm	$(B-r)$	$(V-r)$	R_{50}	ΔR_{50}	$\langle \mu_{50} \rangle$	$\Delta \mu_{50}$	n	Δn	Q	ε_e	ε_{max}	θ_e	$\Delta \theta$	$c_4(r_e)$	c_4^w	$\delta \mu_1$	$\delta \mu_2$
a1		E	23 54 10.1	-10 27 50		17.44	0.06	1.48		1.12	0.11	19.81	0.18	1.60	1.19	0	0.08	0.18	131.3	39.4	0.21	-0.64	1.52	0.85
a2		E/S0	23 54 16.5	-10 27 43		18.10	0.01	1.40		1.07	0.02	20.28	0.02	1.30	0.08	0	0.06	0.15	160.2	71.6	-0.13	-0.05	0.83	1.16
a3		E	23 54 13.5	-10 27 18		18.06	0.02	1.22		0.70	0.03	19.34	0.06	2.50	0.23	0	0.21	0.27	151.1	12.5	1.04	0.30	1.31	1.04
a4		E	23 54 10.7	-10 27 06	0.0761	18.33	0.02	1.39		1.79	0.04	20.83	0.03	2.30	0.22	1	0.09	0.14	133.3	24.9	1.31	-0.18	0.91	0.53
a5		E	23 54 09.0	-10 26 36		18.28	0.11	1.38		0.45	0.10	18.61	0.30	3.20	11.28	0	0.14	0.17	178.8	72.4		0.35	1.72	0.40
a6		E	23 54 15.7	-10 26 30	0.0751	15.96	0.03	1.38		5.56	0.34	21.66	0.08	4.80	0.78	1	0.15	0.24	1.8	22.7	0.20	-0.16	1.24	0.71
a7		E/S0	23 54 23.7	-10 26 27	0.0704	17.23	0.02	1.28		2.43	0.10	21.28	0.06	3.80	0.56	1	0.09	0.16	5.3	117.7	0.27	-0.46	1.28	0.68
a8		Sa/0	23 54 20.9	-10 26 26		19.21	0.04	1.45		0.75	0.05	20.57	0.08	3.10	0.38	0	0.04	0.11	20.3	23.6		-0.37	1.19	0.68
a9		S0/E	23 54 13.8	-10 26 16	0.0811	17.75	0.02	1.48		0.97	0.02	19.71	0.03	7.70	0.22	0	0.19	0.23	156.7	13.7	-0.41	0.40	0.81	0.69
a10		S0/E	23 54 17.2	-10 25 59	0.0715	17.48	0.00	1.46		0.57	0.01	18.24	0.02	9.90	0.41	0	0.18	0.30	0.8	5.6		2.33	1.68	0.81
a11		E/S0	23 54 19.6	-10 25 54	0.0737	17.23	0.03	1.13		2.65	0.19	21.29	0.08	110.00	0.73	1	0.25	0.29	48.4	41.9	0.74	-0.33	1.41	0.51
a12		Sa/0	23 54 09.1	-10 25 42	0.0751	18.26	0.02	1.42		1.58	0.05	21.22	0.05	2.10	0.26	0	0.24	0.33	52.8	89.4	2.08	0.01	0.83	0.77
a13		E	23 54 20.0	-10 25 37	0.0732	17.81	0.04	1.29		1.26	0.09	20.33	0.09	9.90	0.84	1	0.14	0.17	138.2	18.3	0.82	-0.44	1.05	0.60
a14		E/S0	23 54 21.7	-10 25 28	0.0767	17.50	0.02	1.56		1.38	0.04	20.21	0.04	8.20	0.37	0	0.21	0.33	80.7	15.7	1.21	0.97	1.07	0.87
a15		S0/E	23 54 06.3	-10 25 27	0.0746	15.68	0.04	1.40		2.61	0.17	19.92	0.09	2.50	0.59	0	0.44	0.53	12.2	9.3	2.33	0.92	1.19	0.75
a16		E	23 54 07.0	-10 25 17	0.0703	15.79	0.04	1.42		6.47	0.53	21.70	0.11	110.00	2.05	1	0.19	0.32	98.6	14.9	-0.94	-0.12	1.24	0.84
a17		S0p	23 54 21.5	-10 25 11	0.0764	15.87	0.03	1.51		2.01	0.09	19.42	0.06	4.60	0.58	1	0.13	0.37	156.2	9.4	-0.34	-0.39	1.23	0.60
a18		E	23 54 18.4	-10 25 09	0.0733	16.09	0.03	1.43		2.49	0.15	20.10	0.08	7.80	0.66	1	0.11	0.13	35.5	42.4	-0.24	-0.45	1.24	0.73
a19		E	23 54 13.6	-10 25 08	0.0777	13.67	0.03	1.50		19.57	0.93	22.15	0.06	10.00	0.48	1	0.11	0.19	45.9	131.5	0.65	-0.53	1.17	0.61
a20		SB0	23 54 17.1	-10 24 56	0.0819	16.42	0.04	1.47		2.75	0.18	20.64	0.10	4.30	1.22	1	0.25	0.30	123.6	36.8	5.23	0.88	1.40	0.67
a21		S0	23 54 18.0	-10 24 55	0.0771	16.65	0.03	1.44		2.02	0.08	20.24	0.06	2.00	0.38	1	0.36	0.50	89.3	6.2	1.56	0.88	0.95	0.63
a22		E/S0	23 54 04.1	-10 24 51		19.34	0.02	1.47		0.58	0.02	20.17	0.04	2.50	0.32	0	0.05	0.09	113.1	28.1		0.44	1.69	0.38
a23		S0p	23 54 26.0	-10 24 41	0.0841	17.04	0.01	1.48		0.87	0.01	18.76	0.23	1.20	1.67	0	0.04	0.54	175.2	6.4		3.56	1.76	0.55
a24		S0/a	23 54 07.1	-10 24 30	0.0803	18.47	0.06	1.44		0.80	0.09	19.99	0.15	110.00	1.43	1	0.11	0.17	175.0	111.4		0.13	1.63	0.55
a25		Sa/0	23 54 11.2	-10 24 29	0.0818	17.21	0.03	1.41		2.23	0.09	21.06	0.07	2.20	0.49	1	0.28	0.40	85.5	28.7	2.69	0.62	1.10	0.54
a26		SB0	23 54 10.0	-10 24 25	0.0801	16.78	0.05	1.39		3.31	0.32	21.50	0.13	110.00	2.83	0	0.25	0.32	32.7	72.8	0.29	0.52	1.28	0.84
a27		S0	23 54 09.1	-10 24 20	0.0762	16.61	0.03	1.45		1.96	0.06	20.15	0.06	1.20	0.29	0	0.31	0.50	35.0	6.4	1.58	1.36	0.73	0.92
a28		E	23 54 07.0	-10 24 19	0.0750	17.18	0.04	1.42		1.02	0.08	19.26	0.12	2.10	0.81	1	0.05	0.13	156.4	233.8	-0.28	0.07	1.29	0.79
a29		E/S0	23 54 17.0	-10 23 39	0.0765	17.21	0.03	1.43		1.12	0.05	19.52	0.08	.30	0.79	1	0.19	0.30	177.2	38.3	0.55	1.22	1.45	0.79
a30		E/S0	23 54 15.0	-10 23 31		19.28	0.02	1.41		0.80	0.03	20.76	0.06	.70	0.15	0	0.08	0.10	149.1	79.3		-0.32	1.20	1.11
a31		E	23 54 18.9	-10 23 19	0.0781	17.31	0.02	1.32		1.67	0.06	20.52	0.06	1.80	0.29	1	0.10	0.16	18.2	52.3	-0.15	0.01	1.07	0.55
a32		Ep	23 54 13.3	-10 23 10	0.0780	16.01	0.03	1.54		3.41	0.22	20.69	0.08	9.60	0.79	1	0.23	0.30	113.7	14.1	-0.12	-0.57	1.46	0.60
a33		E	23 54 13.7	-10 22 21	0.0809	16.50	0.01	1.50		2.21	0.05	20.18	0.03	4.40	0.27	1	0.16	0.19	171.6	48.4	0.36	-0.37	1.17	0.60

Fig. 12. (a) – Overlap between our CCD fields and DSS imaging for Abell 2151. In Table 6 the fields are listed in ascending order of declination. The galaxies belonging to our sample in each field are marked with small circles. The absolute positions are set by the coordinates (Right Ascension [2000] and Declination [2000]) corresponding to the cross in the plots, while the grid sizes in α and δ are of 30^s and $5'$, respectively. In this figure and in the following ones, relative to the other clusters, the colors of the fields refer to a given telescope+camera configuration: (i) blue for run #1; (ii) green for runs #2 and #3; (iii) orange for runs #4 and #5; (iv) red for runs #6 and #7.

Fig. 12. (b) – Same as Figure 12a, but for Abell 119.

Fig. 12. (c) – Same as Figure 12a, but for Abell 1983.

Fig. 12. (d) – Same as Figure 12a, but for DC 2103.

Fig. 12. (e) – Same as Figure 12a, but for Abell 3125.

Fig. 12. (f) – Same as Figure 12a, but for Abell 1069.

Fig. 12. (g) – Same as Figure 12a, but for Abell 2670.

Abell2151

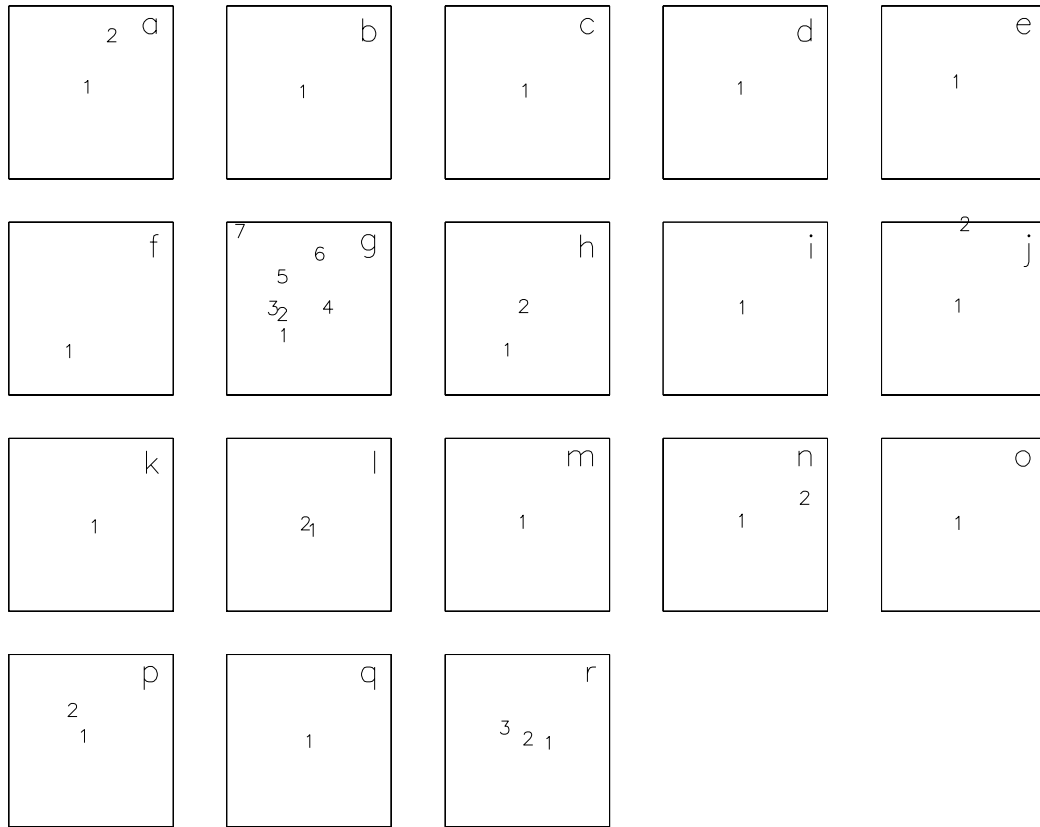


Fig. 13. (a) – Identification of the selected galaxies in our CCD fields of Abell 2151. The galaxies are numbered in ascending order of declination. The alphabetic order of the letters identifying the fields corresponds to the ascending order of declination (see Table 6 and caption of Figure 12).

Abell 119

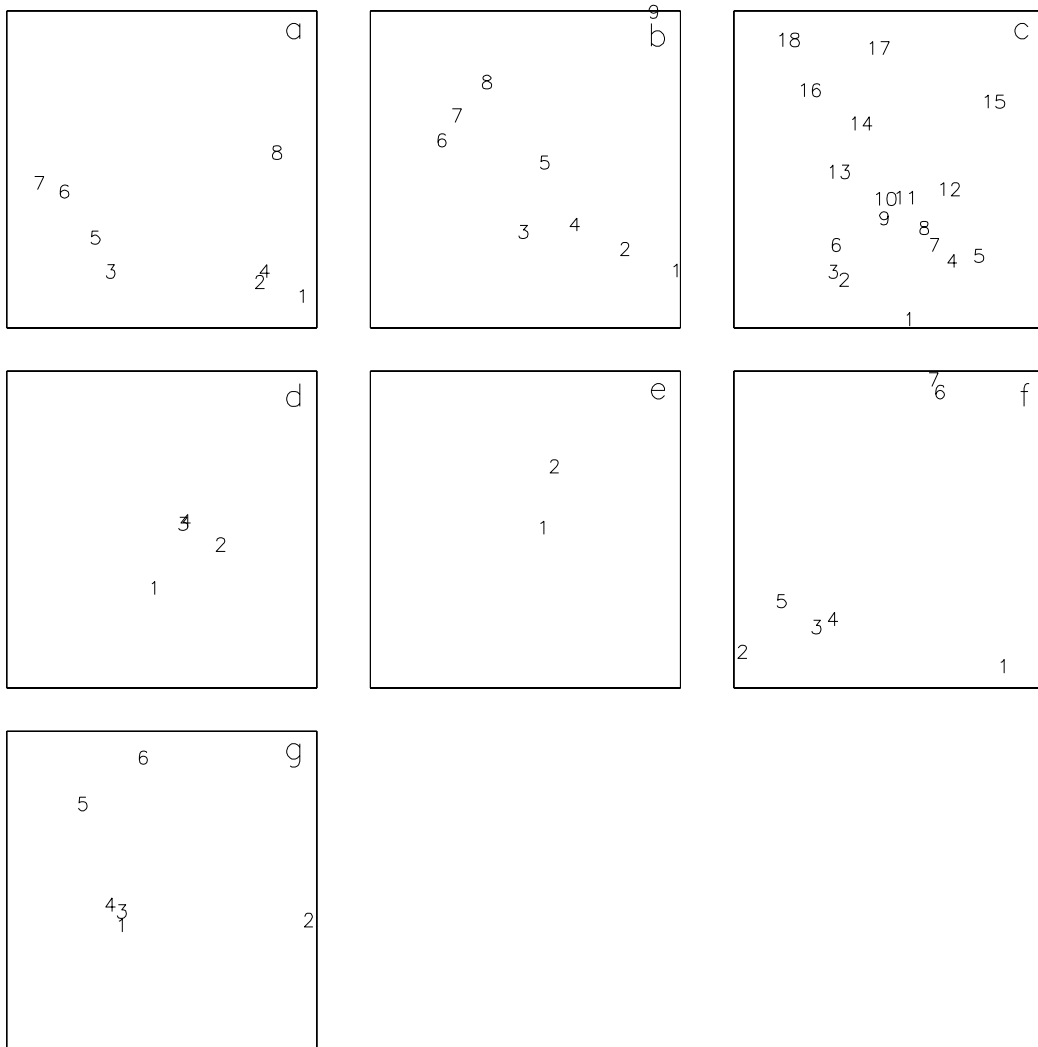


Fig. 13. (b) – Same as Figure 13a, but for Abell 119.

Abell 1983

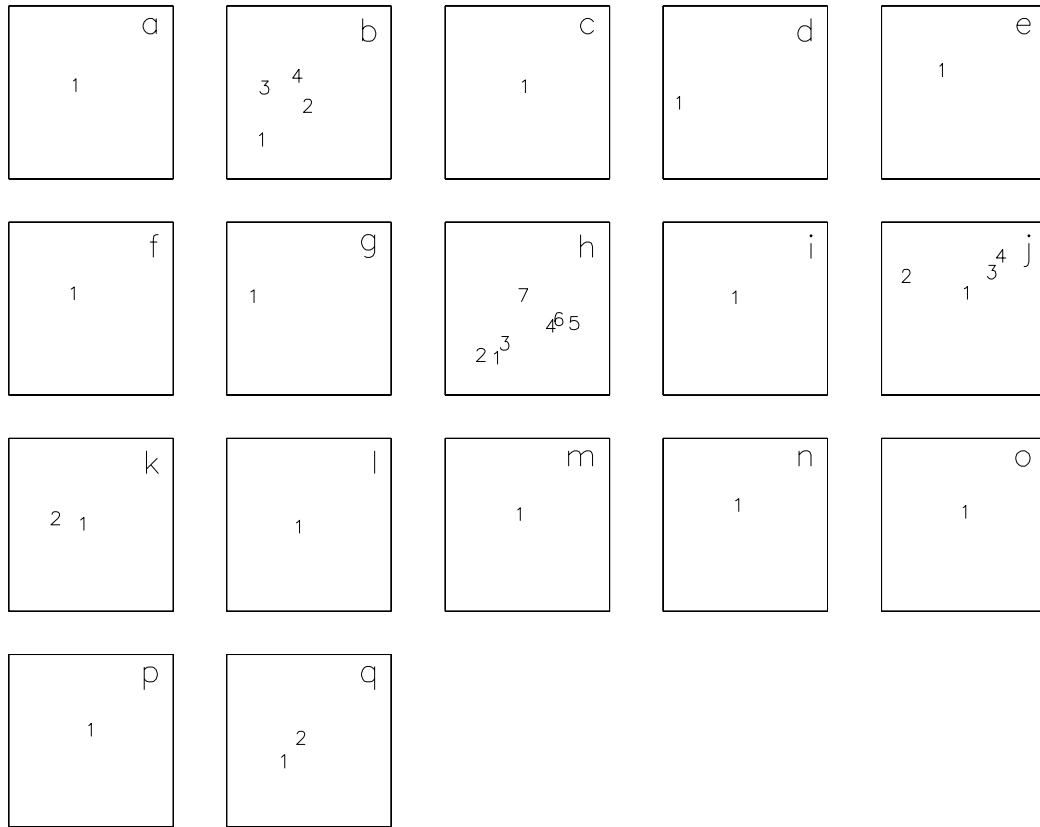


Fig. 13. (c) – Same as Figure 13a, but for Abell 1983.

DC2103

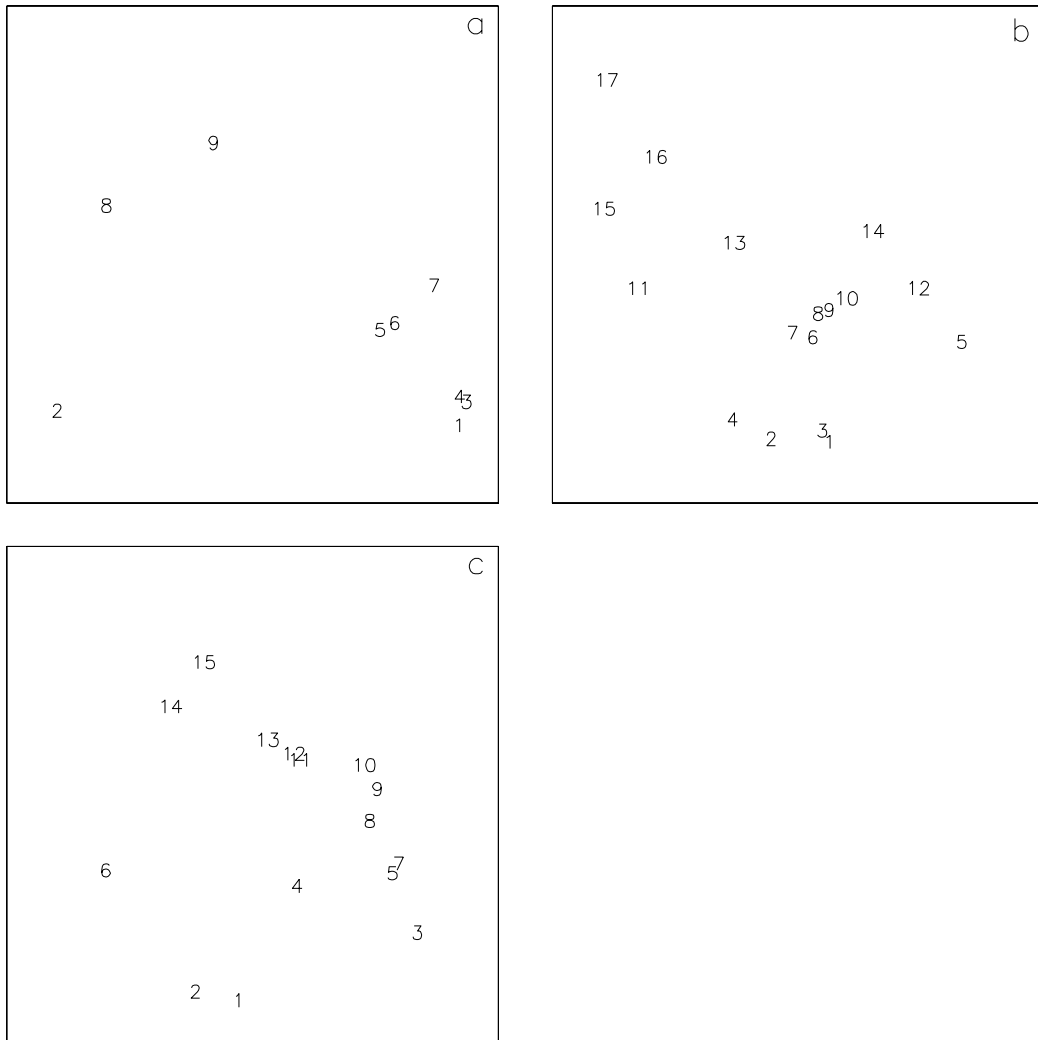


Fig. 13. (d) – Same as Figure 13a, but for DC 2103.

A3125

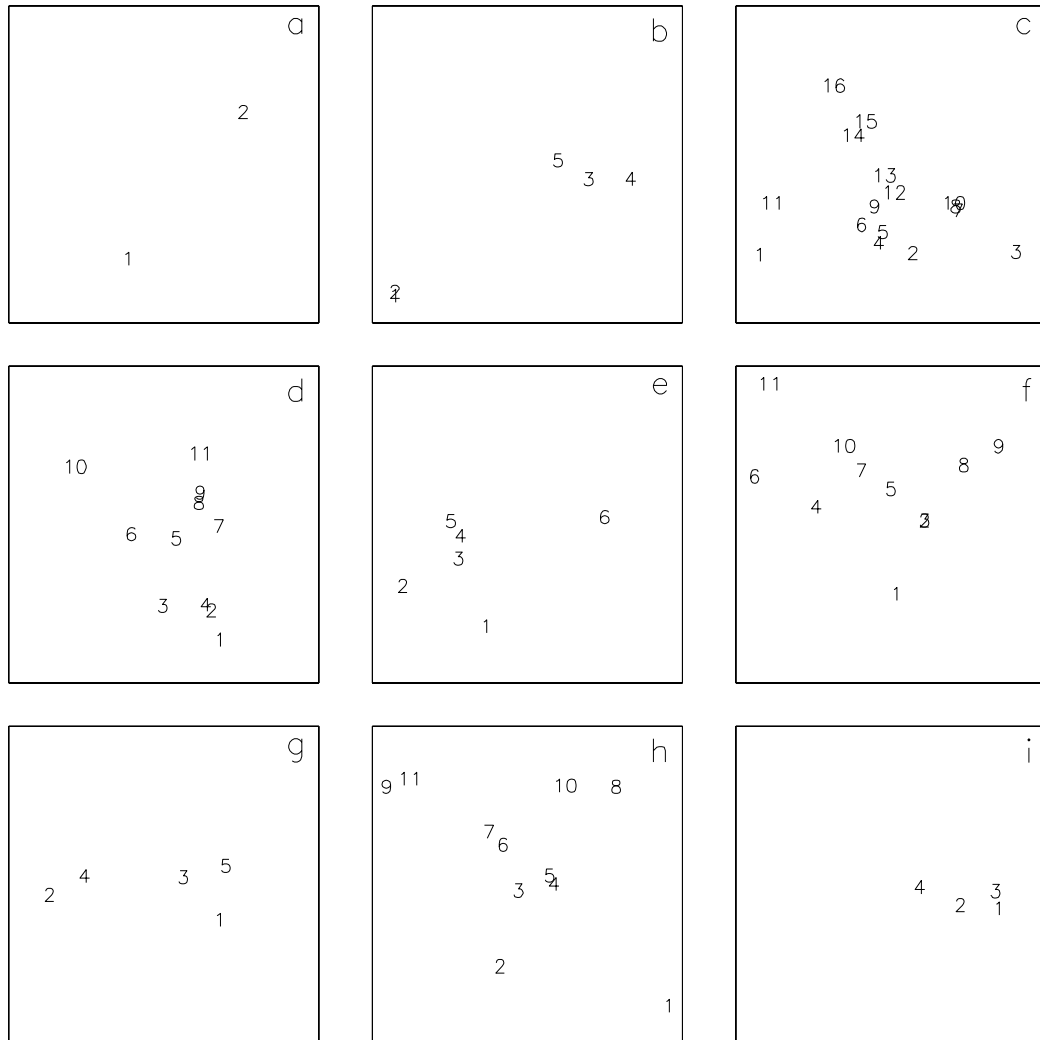


Fig. 13. (e) – Same as Figure 13a, but for Abell 3125.

Abell 1069

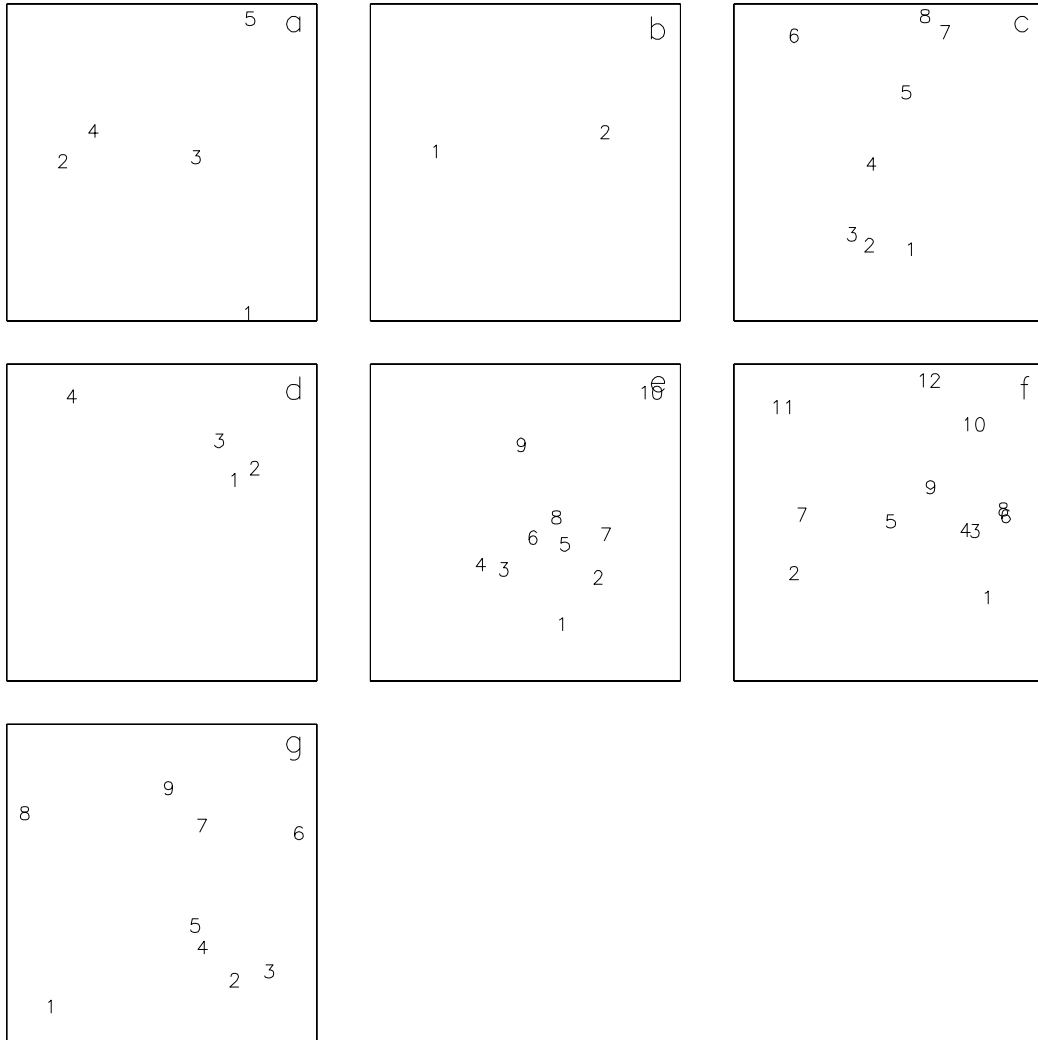


Fig. 13. (f) – Same as Figure 13a, but for Abell 1069.

A2670

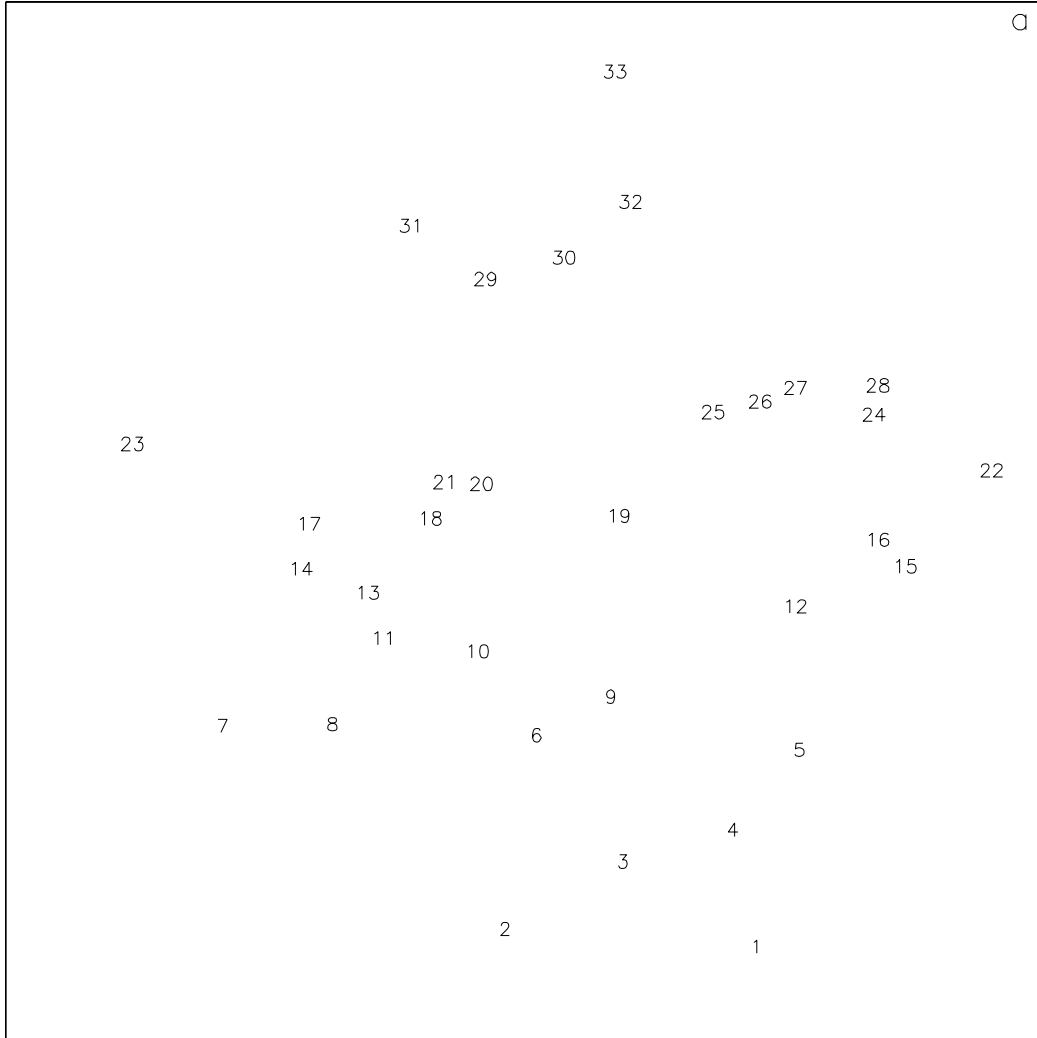


Fig. 13. (g) – Same as Figure 13a, but for Abell 2670.

This figure "fig12a.jpg" is available in "jpg" format from:

<http://arxiv.org/ps/astro-ph/0203013v1>

This figure "fig12b.jpg" is available in "jpg" format from:

<http://arxiv.org/ps/astro-ph/0203013v1>

This figure "fig12c.jpg" is available in "jpg" format from:

<http://arxiv.org/ps/astro-ph/0203013v1>

This figure "fig12d.jpg" is available in "jpg" format from:

<http://arxiv.org/ps/astro-ph/0203013v1>

This figure "fig12e.jpg" is available in "jpg" format from:

<http://arxiv.org/ps/astro-ph/0203013v1>

This figure "fig12f.jpg" is available in "jpg" format from:

<http://arxiv.org/ps/astro-ph/0203013v1>

This figure "fig12g.jpg" is available in "jpg" format from:

<http://arxiv.org/ps/astro-ph/0203013v1>